Devasthal optical telescope - AGN Reverberation Monitoring (DOT-ARM): Probing AGN black-hole masses and broad line regions

Project Completion Report (Grant no: EMR 2016/001723)

1. Principal investigator : Dr. Hum Chand
Scientist-E (on lien),
ARIES, Manora Peak,
Nainital- 263002, Uttarakhand,India

2. Co-Investigator : Dr. Amitesh Omar
Scientist-E,
ARIES, Manora Peak,
Nainital- 263002, Uttarakhand, India

2. Researchers : Dr. Hum Chand
Dr. Amitesh Omar
Mr. Vivek Kumar Jha
Mr. Krishan Chand

4. Implementing institute : Aryabhatta Research Institute of observational sciencES (ARIES), Manora Peak
Nainital- 263002, Uttarakhand, India

A brief summary

The inner regions of Active Galactic Nuclei (AGN) are difficult to resolve even with the modern observation techniques. Yet the knowledge of matter in the sub parsec regions of such objects holds clues to the growth of supermassive black holes even in the earlier epochs of the universe. In the absence of direct observations, indirect time domain techniques such as reverberation mapping have been used by the researchers in the recent past. Through this study, we have attempted to use these indirect techniques to understand the structure and dynamics of matter in the inner regions of active galaxies. We have procured redshifted narrow band filters, to catch the emission line flux arising from the Broad line regions of active galaxies. These filters, reduce the dependency on spectrographs which cost much higher and are complicated enough to be used in smaller telescopes. Using these filters we have applied a technique known as Photometric reverberation mapping which has the potential o yield accurate Black hole masses up to higher redshifts, when the universe was much younger. Further, with broadband observations of a sample of AGN the accretion disk structure has also been studied. The general understanding has been that the AGN accretion disks follow the standard Shakura Sunyaev disk model, but the order of expected lags between the photons coming from the innermost regions of the disk and the reprocessed photons from the outer disk is a few magnitudes large. Only a handful of AGN have precise inter band lag measurements, due to which, observations of a large sample of AGN is a necessity. Through this project, we have

expanded the sample of AGN with the accretion disk sizes significantly and with the incoming data in the upcoming observation cycle, the numbers will increase further. To understand the dynamics of gas in the broad line region, we have made use of the Sloan Digital Sky Survey (SDSS) data for a representative sample of Narrow and Broad Line Seyfert galaxies. The Narrow Line Seyferts have been a peculiar class of AGN with very accretion rates but lower black hole masses. The presence of higher iron content in their line emitting regions adds to their peculiarity. The behaviour of gas in the Broad Line region of such galaxies helps us unveil clues towards this peculiar behaviour. From our analysis we have found a large number of Narrow Line Seyfert galaxies having asymmetric emission line profiles. Moreover, most of the asymmetries are indicative of an outflow component. However, no such peculiarity is seen in the case of Broad line Seyfert galaxies.

The initial aim of this study was to constrain the Broad Line Region radius for a large sample of low luminosity AGN and then proceed towards the modelling of the light curves to yield the geometry of the Broad Line Region. Unfortunately, due to delay in the procurement of filters, the persisting bad weather conditions in the Devasthal observatory hampered our project goals. However, we have readjusted the goals by limiting our sample for emission line reverberation mapping, monitoring the accretion disk through continuum reverberation mapping and unveiling the diverse nature of the Seyfert galaxies. We are continuing the observations of the AGN in our sample and thus we are hopeful that the main objectives of this project to be achieved in the near future.

Contents

List of Figures

List of Tables

Chapter 1

Project details

1.1 Project Title

Devasthal optical telescope - AGN Reverberation Monitoring (DOT-ARM): Probing AGN black-hole masses and broad line region through Photometric Reverberation Mapping (PRM).

1.2 Project Investigators

PI	Co-I	
Dr. Hum Chand Scientist 'E' (on lien) ARIES, Nainital,263002 India	Dr. Amitesh Omar Scientist 'E' ARIES, Nainital,263002 India	

1.3 Implementing institution

Aryabhatta Research Institute of observational sciencES (ARIES)

(An autonomous institute under DST, Govt of India)

Manora Peak, Nainital:263002

1.4 Date of commencement

17 March 2017

1.5 Planned date of completion

16 March 2020

1.6 Actual date of completion

16 September 2020

1.7 Approved objectives of the proposal

- To carry out a AGN-RM program as a major contribution from the observatory which not only fulfills our science goals, but also can cater the need of many broader science goals of the AGN community based on RM data. Here our resources will be optimized with the use of ARIES 1.3m and 3.6m telescopes, along with our own expertise for this purpose.

- To establish a size-luminosity and mass-luminosity relation of AGNs extending it to the low luminosity region for the first time. This we will achieve with a large representative AGN sample covering a wide range of AGN parameter space.

- Use the PRM time delays to get the BH-masses for this sample, and calibrate the so-called single epoch BH-mass measurement method using this representative sample of AGN.

- To establish relationships between BHs and galaxies, since their late-type galaxy hosts do not necessarily contain classical bulges.
- To construct the model to constrain the AGN geometry and kinematics by modeling the observed light curves to search for any effect of luminosity on the BLR geometry.
- Accretion disk modeling from optical U, B, V band monitoring carried out in this experiment.

1.8 Deviations from the approved objectives

- Emission line reverberation mapping campaign for a large sample proved to be challenging. Hence, the accretion disk structure was studied for a sample of sources alongwith the emission line reverberation mapping.
- Archival data from public surveys such as the Sloan Digital Sky Survey (SDSS) and Zwicky Transient Facilty (ZTF) was used.
- The time allocation and the weather at the Devasthal Observatory was not suitable for a large campaign, hence a few other international observatories were involved in the execution of ths project.
- The narrow band emission line RM project is continuing with the involvement of the GROWTH Indian Telescope and Hanle, Ladakh and the JCB Telescope at Kavalur operated by IIA in collaboration with the Devasthal Fast Optical Telscope operated by ARIES.

Chapter 2

Details of Experimental work

In this chapter we present a general introduction to the topic and follow it by the techniques we have developed in order to conduct our experiments. We also present a brief introduction to the telescopes we have used for this project. Finally, we present information about the archival data that has been helpful in achieving our scientific goals.

2.1 A general introduction

In early February 1963, Maarten Schmidt at the California Institute of Technology, recognized that the spectrum of a radio detected source 3C 273 could be interpreted as if the source is located at red-shift 0.16 (e.g., see Schmidt, 1963; Kellermann, 2014). This was the first ever discovered *quasar*, a short form of *quasi stellar source* as it was initially known. Within a few years, a lot of such extra-galactic sources were discovered which since then are known as Active galactic Nuclei or AGN. The term quasar is now commonly used for AGN with high luminosity. Active galaxies differ from normal galaxies by the fact that they are luminous objects which outshine their own host galaxies and the high luminosity arises due to the actively accreting

Super massive Black Hole (SMBH) residing at the centre. This activity provides us observational signature in all the energy bands (see Padovani, 2017; Netzer, 2018). The accretion of matter can be described in the form of optically thick, geometrically thin accretion disk formed in the vicinity of the SMBH (Meyer-Hofmeister et al., 2017).

2.1.1 The AGN Classification

According to the properties of their spectra, AGNs are classified into Seyfert galaxies of type 1 and 2, quasars of type 1 and 2, blazars, LINERs etc.(for comprehensive reviews see Tadhunter, 2008; Netzer, 2015; Merloni, 2016; Padovani et al., 2017, and references therein.)

Seyfert 1 galaxies are the ones showing both broad (of the order of a few 1000 km/s) and narrow emission lines (of the order of a few 100 km/s) in their spectra. Seyfert 2 galaxies have only narrow emission lines in their spectra. Quasars are similar to Seyfert galaxies, but with much higher luminosity. Blazars are defined as those AGN which are characterized by rapid optical variability, high optical polarization, large X-ray and γ-ray luminosity and a variable, flat-spectrum, superluminal radio core (Véron-Cetty & Véron, 2000). BL Lac objects are the blazars which are characterized by a strong continuum and very weak or absent both emission and absorption lines. OVVs are another class of Blazars which are similar to BL Lac objects, with the difference that their spectra are showing strong broad emission lines. LINERs (Low-Ionization Nuclear Emission Line Regions) are the least luminous and the most common AGNs. Approximately one third of all nearby galaxies may be classified as LINER galaxies. However, it remains uncertain whether all LINERS are truly AGN, or rather a subset of them represent nuclear star forming regions. In terms of spectra, the narrow lines arising out of LINERs are clearly distinguished from that of the Seyfert galaxies, showing a lower degree of ionization.

The classification of AGN into various sub-types is influenced by their orientation with respect to the observer. Depending on the orientation at which this structure is viewed, different spectral signatures are seen. In particular, the broad emission line region is only visible to observers with a relatively face-on view. If viewed from the side, the torus blocks the same and only narrow emission lines will be seen in the AGN spectrum.

2.1.2 Components of AGN

Supermassive Black Holes (SMBH) are understood to be the central part of an AGN. The SMBH accretes matter and is surrounded by a disk composed of the in falling matter. Observationally, the accretion disk is the closest part to the SMBH of any AGN. Relativistic jets are launched from the accretion disk itself (Gourgouliatos & Komissarov, 2018). If magnetic fields are present, they are likely to rip away parts of the ionised gas from the accretion disk, and force it to move according to the field. The matter particles are flung out in space to large distances, such that the jets can extend past the rest of the galaxy. The jets also become the area for the strongest radio emission.

Right outside the accretion disk, are clouds of gas that are dynamically strongly affected by the SMBH. These clouds have emission lines which are observed to be broadened to an order of a few 1000 km/s (see Bentz et al., 2006; Li et al., 2016, also see section 2.1.3). While the radio jets can easily extend beyond the rest of the galaxy, the gas clouds are within light days from the SMBH (see Kaspi et al., 2002). The energetic photons streaming from the accretion disk ionise the clouds, and the strong gravitational pull forces the clouds to move at high speeds to maintain their orbits. At a certain distance from the SMBH, the flux is small enough for neutral regions to exist. Photons reaching these regions may partially photon ionise the clouds, resulting in a cascade of recombination lines.

Dust particles such as graphite cannot survive in regions with strong ultraviolet (UV) radiation; they evaporate if located in a place where the equilibrium black body temperature above approximately 1500 K. The radius at which graphite can exist is called the dust sublimation radius, and it is considered to be the starting point of the so-called obscuring/dusty torus (see Ramos Almeida & Ricci, 2017). The presence of dust is significant in AGN, as it is in other areas of astronomy. In the unified AGN model it provides the opacity needed to hide the central parts of the AGN if observed at the right angle, leading us to observe seemingly different active galaxies.

The narrow line region (NLR) is made up of interstellar gas, which is less dense than that of the BLR (see Netzer, 2008). The region is also larger, and extends much further from the BH. As the name suggests, the emission lines from this area are more narrow (of the order of a few 100 km/s) than those from the BLR, which is a consequence of the larger distance from the BH. Both permitted and forbidden emission lines are observed to arise from this region. Permitted emission lines are emission lines occurring readily on Earth and other high density environments. Forbidden emission lines correspond to low probability transitions from meta stable energy levels in atoms. The low probability leads to a long lifetime for the transitions, and in sufficiently high density regions the energy is carried away by atom collisions before the low probability transition may occur. With a larger distance to the SMBH, the broadening of the emission lines is not equally strong in the narrow line region, resulting in both the permitted and forbidden narrow emission lines.

2.1.3 The broad line region (BLR)

As already mentioned, gas right outside the accretion disk is observed to have emission lines broadened to an order of 1000 km/s (Bentz et al., 2006; Li et al., 2016). This region is known as the Broad Line Region (BLR). This region is of research interest as it is one of the most characteristic features of Active Galaxies, but the

mechanism responsible to emit these strong lines is not clear. How gas in the BLR is moving, whether it is inflow (as suggested by Gaskell & Goosmann, 2016), outflow, or orbital motion, around the central object remains unknown. BLR offers prospects to measure the absolute luminosity of the source in a way which is independent of the red shift either by identification of the sources emitting close to Eddington ratio or by combining the measured size and the theoretical R-L scaling. How the BLR forms is still an unanswered question in the field of Active Galaxies (Czerny, 2019). Direct observation of this region in the optical regime is observationally difficult, as it projects to sub-microarcsecond angular resolutions, which is not resolvable by any present or near future observational facilities. But since the AGN are highly variable, time resolution substitutes for the spatial resolution. Through a technique known as Reverberation Mapping (RM)(Bahcall et al., 1972; Blandford & McKee, 1982; Peterson & Horne, 2004; Bentz, 2015, see section 2.1.4) the extent of this region from the central engine of the AGN can be estimated.

2.1.4 Reverberation Mapping

RM makes use of the intrinsic variability of the continuum source in active galactic nuclei to map out the distribution and kinematics of line-emitting gas from its light travel time-delayed response to continuum changes.

to estimate the distance between two objects by mapping out the response of the emission lines to the ionizing continuum. It uses the time resolution instead of angular resolution (Bentz et al., 2013) to determine the distance of two sources. Also known as echo mapping, this technique is similar to the bats using the echo to obtain the distances to their targets. RM remains the primary method to probe these inner regions of the Active Galactic Nuclei. RM makes use of the intrinsic variability of the continuum source in active galactic nuclei to map out the distribution and kinematics of line-emitting gas from its light travel time-delayed response to continuum

changes. As with any other technique, a few assumptions are made before successful reverberation mapping is performed:

- The continuum originates from a single central source.
- Light travel time is the most important time scale.
- There is a simple, though not necessarily linear, relationship between the observed continuum and the ionizing continuum.

The emission lines respond to the continuum variations with a lag and by estimating this lag, the distance of the region emitting emission lines, in this case the BLR, could be determined from the central ionizing source. The emission lines respond to the ionising continuum in the following manner:

$$s_l(t, V) = \int d\tau . \psi(\tau, V) . s_c(t - \tau) \tag{2.1}$$

where $s_c(t, V)$ is the continuum line light curve, $s_l(t, V)$ is the emission line light curve, $\psi(\tau, V)$ is known as the *transfer function* or the *velocity delay map* (Zu et al., 2011) and V is the line-of-sight velocity. The emission line lag (τ) is estimated using cross correlation of the light curves. Basically the mean BLR size, R_{BLR} obtained will be : $R_{BLR} = c\tau$ where (c) is the speed of light and (τ) is the lag obtained between the continuum and emission line variations. The fundamental goal of all reverberation mapping campaigns is to obtain this lag between the emission line and the continuum which is the first moment of the transfer function $\psi(\tau, V)$. The estimated *lag* usually of the order of a few light days although Edri et al. (2012) obtained a reverberation lag as low as 3.5 hours for an AGN as well. RM provides the only direct observational estimate of the spatial extent of the BLR. But, the campaigns are lengthy, targeted and quite resource consuming (Netzer & Peterson, 1997). Due to these factors, the reverberation based studies have been carried out for

about a hundred sources so far, a number quoted by Czerny (2019) but, with multi object reverberation mapping campaigns ongoing (see section: 2.2) this number will surely increase manifold in time to come. The size of the BLR can be used to estimate the mass of the Black Hole M_{BH} using the following virial relation, if the Doppler width $\triangle V$ of the emission line is known:

$$M_{BH} = \frac{f \triangle V^2 R_{BLR}}{G} \tag{2.2}$$

where R_{BLR} is the size of BLR obtained through reverberation mapping, G is the universal gravitational constant and f is a dimensionless correction factor (Du et al., 2015). The mean value of this dimensionless correction factor depends on the geometry and inclination of the region and its exact values remains a matter of debate. In the literature,different values for f have been used ranging from 2 to 5, based on estimates of the BH mass through other means.

An empirical relation linking the size of the BLR to the luminosity of the AGN, the so called R-L relation (Bentz et al., 2013) has been obtained and research has been going on to validate this relationship at all luminosities . In the traditional reverberation mapping scenario, the spectrum being obtained for RM is both resource and time consuming and which is quite a challenging task to execute on 1-2 m class telescopes which are already loaded with a wide variety of proposals. Thus an option is to obtain both the continuum and emission line flux using a combination of broad and narrow band filters itself. This technique is known as Photometric Reverberation Mapping (PRM). PRM uses one band to trace the continuum and another narrow band to trace the emission line, but needs much less telescope time than the spectroscopic RM and can be also done with smaller 1-2m class telescopes. The ARIES Devasthal Optical Telescope - AGN Reverberation Monitoring (DOT-ARM) (see Chand et al., 2018) project utilizes the concept of PRM and is aimed

at the study of nearby low luminosity AGN having luminosities $L < 10^{43}$ ergs/s. This regime has not been explored fully in the past campaigns. 8 narrow band filters with their central wavelengths falling at redshifted $H\alpha$ and $H\beta$ wavelengths have been procured to obtain the emission line flux. A sample of carefully selected AGN has been chosen with redshift such that they fall in range of the filters. PRM has been demonstrated as a successful alternative by Haas et al. (2011) and Chelouche & Daniel (2012) in their recent works. A few sources studied using PRM are mentioned below and the lags obtained are in good agreement with the spectroscopic lags.

2.2 Review of the Literature

Reverberation mapping has become the primary technique to study of the kinematics and geometry of BLR, as well as in measuring the masses of SMBHs residing at the centers of AGNs Reverberation mapping campaigns have continued ever since the technique was explored by Bahcall et al. (1972) and Blandford & McKee (1982). The International AGN Watch Consortium[1] (Netzer & Peterson, 1997; Peterson, 1999) was the first ever systematic campaign for the reverberation mapping of a number of AGN. It combined ground and space based monitoring of 11 different AGN and obtained BLR sizes for all of them and the data is available for the public.

Due to the limitations of telescope time and instrumentation the RM campaigns are restricted to monitoring small numbers of AGN using relatively small telescopes for relatively small time-scales. The Lick AGN Monitoring Program (LAMP-2008) [2] started in 2008, was a dedicated 64-night spectroscopic monitoring campaign with the aim of measuring the masses of the black holes in 12 nearby ($z \leq 0.05$) Seyfert 1 galaxies using the Lick Observatory 3-m Shane telescope and supplemented by four small-aperture telescopes employed in photometric monitoring (Bentz et al.,

[1]http://www.astronomy.ohio-state.edu/ agnwatch/
[2]https://www.physics.uci.edu/ barth/lamp.html

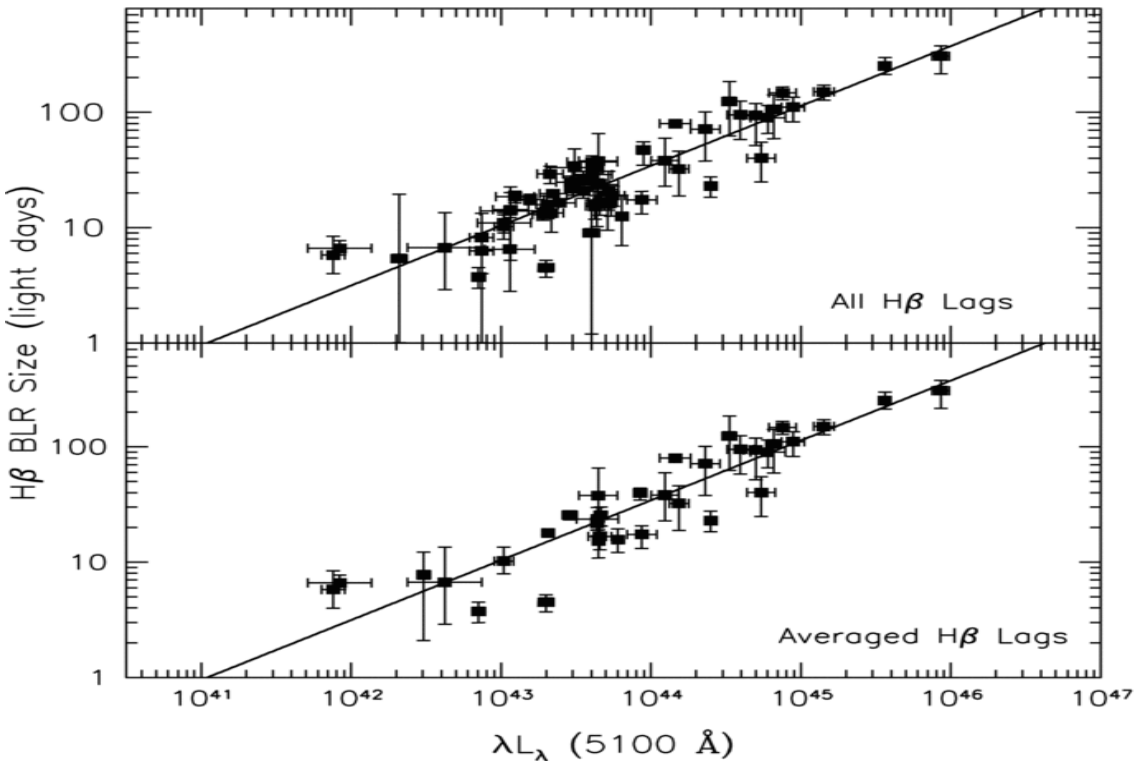

Figure 2.1: The Radius-Luminosity (RL) relation for the AGN

2009, 2010). In 2011, the project was executed again as LAMP-2011 in a 2.5 month reverberation mapping campaign using the 3 m Shane telescope at Lick Observatory, monitoring 15 low-redshift Seyfert 1 galaxies (Barth et al., 2015).

Sloan Digital Sky Survey Reverberation Mapping (SDSS-RM) project (Shen et al., 2015) has been started as a dedicated RM campaign that simultaneously monitors 849 quasars with spectroscopic baseline of 7 years and photometric baseline of 10 years. It is the largest reverberation mapping campaign undertaken till date. A few results have already been published with the data collected so far (see Grier et al., 2018; Homayouni et al., 2018; Yue et al., 2018; Grier et al., 2019; Hemler et al., 2019; Shen et al., 2019; Wang et al., 2019). The OzDES survey has been started as a spectroscopic counterpart to the Dark Energy Survey (DES) (King et al., 2015). It is repeatedly monitoring the DES fields at the Anglo-Australian Telescope (AAT). A number of fibres in each field have been dedicated to monitoring a select group

of quasars to perform RM. OzDES aims to monitor approximately 500 quasars in a timeline of 5 years and recover successful reverberation lags.

The AGN Space Telescope and Optical Reverberation Mapping (STORM) project monitored NGC5548 in multiple wavelengths. The AGN STORM campaign is anchored by daily far-UV observations using the Cosmic Origins Spectrograph on the Hubble Space Telescope (HST) (see (De Rosa et al., 2015)). A large reverberation mapping (RM) campaign targeting super-Eddington accreting massive black holes (SEAMBHs) in active galactic nuclei (AGNs) is being executed using the 2.4-m Shangri-La telescope at the Yunnan Observatory (see Du et al., 2014; Wang et al., 2014; Du et al., 2016, 2018).

NGC 5548 has been one of the most intensively observed objects for reverberation mapping. It has been monitored at least by 19 individual campaigns, including the International AGN Watch Consortium ((Peterson, 1999), the Lick AGN Monitoring Project (LAMP)-2008 (Bentz et al., 2009), and the AGN Space Telescope and Optical Reverberation Mapping (AGN-STORM) project (see De Rosa et al., 2015; Bon et al., 2016) presented an analysis of 43 years of spectroscopic observations for the same object signifying how intensively this AGN has been monitored over time.

By virtue of these reverberation mapping campaigns, a relation between the size of the BLR (R) obtained through reverberation mapping of the $H\beta$ line and the luminosity of the AGN has been obtained:

$$log(R_{BLR}) = K + \alpha.log(\lambda L\lambda(5100\mathring{A})) \tag{2.3}$$

This relation is quite tight with a power-law slope of $\alpha = 0.665 + 0.069$ (Bentz et al., 2009) (also see Figure 3.7).

PRM has been a relatively new technique and a large systematic project on the lines of the ones mentioned above has not been undertaken yet. Introduced by

Haas et al. (2011) and Chelouche & Daniel (2012), monitoring of sources through PRM has been restricted to single object campaigns for majority of the time. A campaign for 3C120 has been reported Pozo Nuñez et al. (2012) and NGC 4395 has been monitored using broadband filters by Edri et al. (2012). Nuñez et al. (2017) present an ongoing systematic PRM performed using narrow band filters at the WISE observatory. Zhang et al. (2017a) have published results using PRM for a few sources selected out of quasars from the SDSS-Stripe 82 catalogue. In our country, there have not been much effort to carry out RM experiments due to unavailability of large telescopes and only recently with the installation of telescopes such as the 1.3m and 3.6m telescopes[3][4] at the Devasthal Observatory, such campaigns have been deemed feasible. Mandal et al. (2018) have recently reported dust reverberation mapping using 2m Himalayan Chandra Telescope (HCT). People have used the RM results obtained by other international groups as an empirical relation based on the calibration of RM results. In this regard, a PRM campaign from this observatory will significantly help in understanding the low luminosity AGN population and their neighbourhood. In the near future, Large Synoptic Survey Telescope(LSST) will monitor the large sky areas in 6 broad bands with a photometric cadence of 3-4 days (MacLeod et al., 2010). This will bring us a unique opportunity to obtain the BLR sizes for hundreds of AGNs/quasars with PRM (Haas et al., 2011).

PRM of the $H\beta$ or $H\alpha$ line is limited to z $\leq$ 1 in the optical regime, as at larger red-shifts these lines fall in the infrared (IR) regime. The MgII emission line falls in the optical regime at these red-shifts but the line is not very strong hence reverberation mapping using this line is very difficult. Thus the potential of PRM in the optical domain is limited to lower red-shifts. If one targets low luminosity AGNs at lower luminosities as well, the area is relatively unexplored as well as under

[3]https://www.aries.res.in/ 1.3m/ariesmain.html
[4]https://www.aries.res.in/dot/

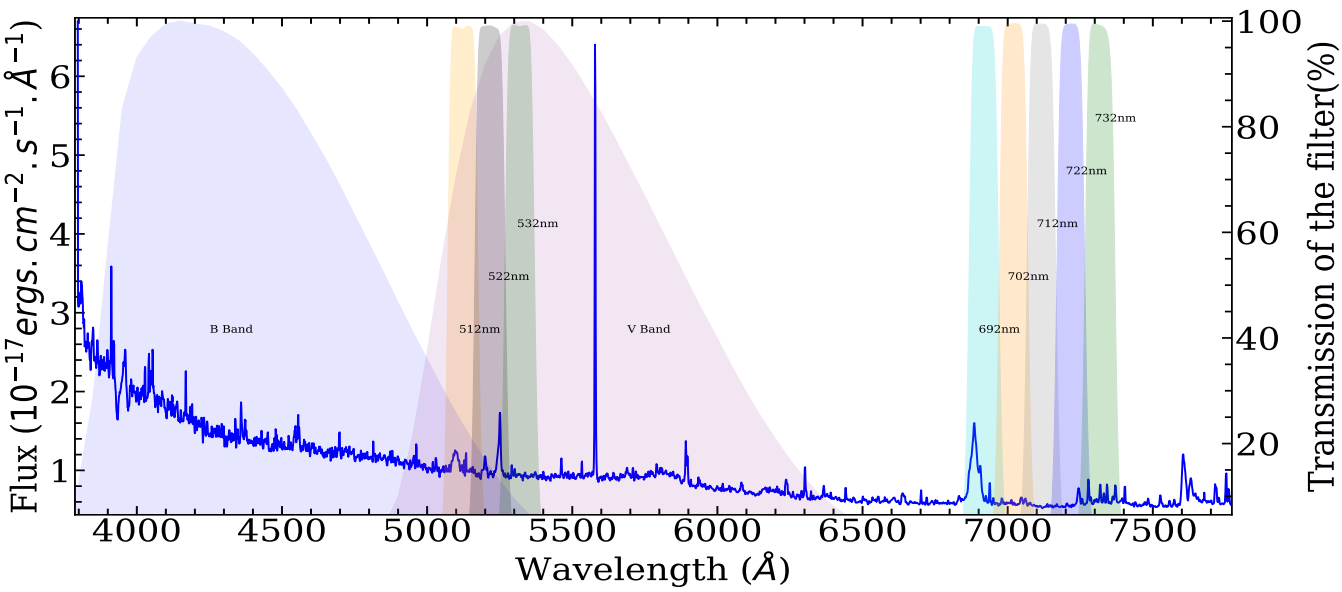

Figure 2.2: The transmission curve of the recently procured 8 narrow band filters covering Hα and Hβ emission lines.

sampled.

2.3 Procurement of narrow band filters

Reverberation mapping requires continuous monitoring with optimum cadence for a duration much longer than the reverberation time scales. Thus, multi epoch continuum and emission line light curves need to be prepared. Since, for PRM the imaging observations need to be done, 8 narrow band filters (see Figure 2.2) having central wavelengths (512nm, 522nm, 532nm) for $H\beta$ and (692nm, 702nm, 712nm, 722nm, 732 nm) for $H\alpha$ were procured to cover the emission lines at various redshifts. A grant of Rs 25,22,780 was available to purchase the redshifted narrow band Hα and Hβ filters. These red-shifted filters are highly specific, and due to various administrative and technical circumstances we had to re-tender it many times. As a result till the beginning of 2018, we could not place the order for the filters, causing in the delay in execution of our project. The filters arrived in the second week of July

2018. They were placed in the available filter slots at 1.3m DFOT. The observations started in the cycle commencing October 2018. A sample of low luminosity AGN with $L_{5100} < 10^{43}$ ergs/sec (L_{5100} is the luminosity measured at 5100 Å) and redshift less than 0.1 from the SDSS DR-VII (Sloan Digital Sky Survey- data Release VII) was monitored using the observational facilities listed below.

2.4 Lag estimation methods

Through the method of reverberation mapping the aim is to estimate the reverberation lags between $H\alpha$ or the $H\beta$ lines coming from BLR clouds and the continuum assumed to be coming from the accretion disk. Thus, it becomes extremely necessary to develop a method which helps us do so in a robust, comprehensive and error minimizing manner. From the review of the literature we obtained two robust methods: the Interpolated Cross Correlation (ICCF) method developed by Peterson et al. (1998) and the recently publicly available JAVELIN [5] code by Zu et al. (2011). The ICCF method cross-correlates the linearly interplolated light curves and gets the lag as the peak of the cross correlation function. For the estimation of lags through ICCF we obtained its Python implementation (PyCCF) [6]developed by Sun et al. (2018); Peterson et al. (1998).

2.4.1 Lag estimation using JAVELIN

We use the publicly available code JAVELIN developed by Zu et al. (2011, 2013). The code models the variability of the AGN as a Damped Random Walk (DRW) or in other terms an Ornstein Uhlenbeck (OU) process for timescales longer than a few days. This approach has been demonstrated by Kelly et al. (2009) and MacLeod

[5]https://www.bitbucket.org/nye17/javelin
[6]http://www.ascl.net/code/v/1868

et al. (2010) where they applied the same model to a large number of quasar light curves. The covariance function for this DRW process takes the following form:

$$S(\triangle t) = \sigma_d^2 e^{(-|\triangle t/\tau_d|)} \tag{2.4}$$

where $\triangle t$ is the time interval between the two epochs and σ_d and τ_d are the amplitude and the time scale of variability respectively. Only these two parameters play a role in the variability of the quasar. Lag estimation in JAVELIN is based on the the ansatz that emission line variability is a scaled, smoothed and displaced version of the continuum. Initially, it builds a continuum model to determine the DRW parameters σ_d and τ_d of the continuum light curve. Then JAVELIN assumes that the emission line lightcurve, is a shifted, smoothed and scaled version of the first lightcurve. This fits three additional parameters for emission lines: the time lag, the top hat smoothing factor and the flux scaling factor (Yu et al., 2018). Once the posterior distribution of the DRW parameters is derived, we have a pretty good idea of how much the continuum light curves in unobserved epochs should vary relative to observed epochs, i.e., we know how to statistically interpolate the continuum light curve. To measure the lag between the continuum and the emission light curve, JAVELIN then tries to interpolate the continuum light curve based on the derived posteriors, and then shifts, smooths, and scales each continuum light curve to compare to the emission line light curve. The continuum and emission lines are convolved using a top hat transfer function having the form:

$$\psi(t - t') = A(t_2 - t_1)^{-1} \tag{2.5}$$

for $t_1 \leq t - t' \leq t_2$

After doing the shifting, smoothing and scaling many times in a MCMC run, JAVELIN finally derives the posterior distribution of the lag t, the tophat width w, and the scale factor s of the emission line, along with updated posteriors for the timescale τ_d and the amplitude σ_d of the continuum. JAVELIN uses the kick-ass MCMC sampler named emcee. Emcee works by randomly releasing numerous walkers at every possible corner of the parameter space, which then collaboratively sample the posterior probability distributions. The number of walkers, the number of burn-in iterations, and the number of sampling iterations for each walker are specified by nwalker, nchain and nburn respectively. In practical usage,the number of walkers, the chain length, as well as the burn-in period of the MCMC, had to be increased many times the default value in order to converge to a single value of the lag.

2.4.2 Lag estimation using ICCF method

The Interpolated Cross Correlation Function (ICCF) Method is the more traditional method to obtain the lags. In this method, first, one adopts a model light curve that is supposed to drive the other variations. The driving light curve is then convolved with a transfer function (equation.1) that produces a responding light curve, which most often represents the response of a broad emission line to the continuum variations. The driving and responding light curves are then sampled in a fashion that somehow mimics the real observations, and then the effects of observational uncertainties, both random and systematic, are included. These artificial data sets are then cross-correlated as if they were real data, and the cross correlation lag (based on either the peak or the centroid of the cross-correlation function) is recorded. The strength of the correlation is given in terms of the *correlation coefficent (r)*:

$$r = \frac{\sum_{i=1}^{N}(x_i - \bar{x})(y_i - \bar{y})}{\sqrt{\sum_{i=1}^{N}(x_i - \bar{x})^2}\sqrt{(y_i - \bar{y})^2}} \tag{2.6}$$

where there are N pairs of values of x and y and $\bar{x}$ and $\bar{y}$ are the mean values respectively. It is obvious that the correlation between the continuum and emission-line flux is even better if a linear shift in time between the emission and the continuum light curves is allowed. This is what cross-correlation does.This process is then repeated a large number of times to build up a cross-correlation peak distribution (CCPD) and the cross-correlation centroid distribution (CCCD)(Peterson et al., 1998).

Since the lag is determined from the peak (or the center of gravity) of the CCF, which is the convolution of the ACF with the transfer function, the required accuracy is a small fraction of the CCF width. There are several methods of determining the CCF, but none with a rigorous way of estimating the associated uncertainty. Thus, a slight misjudgment of the center of the asymmetric CCF gives a large uncertainty on the lag(Netzer & Peterson, 1997). The uncertainities in estimating lags arise due to two primary reasons: (a) flux uncertainties in individual measurements and (b) uncertainties associated with the observational sampling of the light curves, i.e., the intervals between observations and the duration of the experiment.

We have used a python implementation of the same code developed by Peterson et al. (1998); Sun et al. (2018). This method requires the range of the lag which is to be estimated to be put as well as the interpolation frequency, which is usually set to 1 day for well sampled data sets. Basically, it means the interval at which it interpolates between the irregularly sampled data to make the continuous light curves. Next, the number of Monte Carlo iterations for calculation of uncertainities is required (we set it to 500), the MCMC mode, which provides us with two options: either Flux Redistribution (FR) or the Random Subset Selection (RSS) sampling and, the threshold for considering a measurement significant which we set it to 0.5 which basically meant it rejected all CCF with $r_{max} \leq 0.5$.

2.5 The sample of AGN studied

A sample of 54 low luminosity, Type 1 AGN, which have not been reverberation mapped previously with either spectroscopic or photometric techniques was initially selected from the Sloan Digital Sky Survey-Data Release 7 (SDSS-DR7) (cite Greene and Ho) (see table). These are type 1 AGN with prominent $H\alpha$ and $H\beta$ emission lines. The redshift range of the sources has been taken to be 0.01 to 0.1 based on the coverage of our narrow band filters. We have given preference to radio loud AGN over radio quiet AGN as they have been observed to show more variability compared to radio quiet ones (put citations here).These sources have been selected based on visibility at our location, bolometric luminosities ($L_{5100} \leq 10^{43}$ ergs sec^{-1}) and redshift distribution. We obtained the single epoch SDSS spectrum for each source and calculated the FWHM of the $H\beta$ line and the luminosity at 5100Å. These two parameters are used to estimate the empirical BLR size and the SMBH mass respectively. The expected BLR size from the radius-luminosity scaling relation of these sources is of the order of a few days.

One major advantage of narrow band filters is that the contamination from the host galaxy as well as the continuum as experienced in the broad band photometric reverberation mapping campaigns is reduced significantly. The flux obtained in the narrow band filters contains the emission line prominently with contribution from the underlying continuum , which can be reduced by placing a narrow band filter on either side of the emission line profile. The sources were monitored with approximately 2 day cadence, using the narrow band filters for $H\beta$ and $H\alpha$ emission lines and the broadband B and V band Johnson's filters for the continuum. We put a narrow band filter in another slot which obtained the flux from the emission line free region. Besides, for studying the accreiton disk structure, we used the UBVRI filters to get the broadband flux.

2.6 Telescopes used

We primarily used the 1.3m Devasthal Fast Optical Telescope (DFOT), installed at Devasthal Observatory in Uttarakhand India. Broadband B and V band observations were complemented using the 1.04m Sampoornand Telescope (ST) located at Manora Peak, Nainital, India. But unfortunately, the weather condtiond throughtout the observg seasons of 2018 and 2019 were not conducive for large campaigns. We thus, reached out to other observatories in the world to share telescope time with us. We approached the international telescope facilities such as the South African Astronomical Observatory (SAAO) in South Africa, The Skinakas Observatory in Greece, the Xinglong observatory in China and the National Astronomical Research Institute of Thailand (NARIT). We managed to get sufficient telescope time at the 85cm telescope of the Xinglong observatory and at NARIT. Apart from the 1.3m DFOT, this project utilized the data from 85cm telescope at the Xinglong observatory [7] and the network of Thai Robotic Telescopes (TRT)[8] operated by NARIT, Thailand.

2.7 Archival data used

For a part of this project we made use of the Sloan Digital Sky Survey (SDSS)[9] and the Zwickey Transient Facility (ZTF)[10] archival data. SDSS is a dedicated imaging and spectroscopic survey using the 2.5m telescope at the Apache Point observatory. The spectra are taken using two spectrographs. A dedicated set of 640 fibres covering a wavelength range of 3800-9200 Å is used for the SDSS spectrograph and a set of 1000 fibres covering a wavelength range of 3600-10400 Å is used for the Baryon

[7] http://www.xinglong-naoc.org/html/en/
[8] https://trt.narit.or.th/
[9] https://dr16.sdss.org/
[10] https://www.ztf.caltech.edu/

Oscillation Spectroscopic Survey (BOSS) spectrograph (see Smee et al., 2013, for more information.) SDSS IV is the most comprehensive database yet and the latest data release (SDSS DR 16) contains spectra for 750,414 confirmed quasars. More information about the SDSS database of spectra is available in (York et al., 2000; Abazajian et al., 2009; Shen et al., 2011a; Rakshit et al., 2017; Lyke et al., 2020, etc.).

ZTF is a time domain survey which is being run by reusing of the Palomar 48 inch Samuel Oschin Schmidt Telescope. ZTF is designed to prepare ground for the data arriving from the future Large Synoptic Survey Telescope (LSST). ZTF monitors a particular filed with high cadence using three custom filters, ZTF-g, ZTF-r, and ZTF-i . The final design achieves more than an order of magnitude improvement in survey speed relative to PTF, an earlier version of the survey using the same telescope. A fraction of the data set is available for public usage. More information about the ZTF survey is available in (Patterson et al., 2019; Bellm et al., 2019, etc.)

Chapter 3

Results

In this chapter we present the various results obtained from the project so far. First, we present the results of feasibility study carried out using 1.3m DFOT before the arrival of narrow band redshifted filters. Next, we present the results of the calibration of the technique of Photometric Reverberation mapping with the traditional Spectroscopic reverberation mapping. In the next section,we present the emission line delays and the Black Hole mass obtained for SDSSJ115138.1+561331.8. After that, the results obtained from the accretion disk lags for a set of quasars is presented. We then present the ongoing observations using the network of Thai robotic telescopes (TRT) for which the observations are complete. Finally, we conclude with the results obtained by studying a large section of Narrow and Broad Line Seyfert galaxies using publicly available SDSS data.

3.1 Feasibility study for Photometric Reverberation Mapping

The 1.3m DFOT has OIII and SII filter in place. The OIII filter covers a wavelength range of 100Å near the OIII wavelength doublet [4957-5007 Å]. The idea of the

feasibility study was to select an AGN with such redshift that the Hβ emission line falls in this filter. We managed to select one AGN for this study.

3.1.1 Observations

The source, we have chosen for this feasibility study is a nearby low luminous AGN MCG+09-16-013 having at J2000 RA and Dec as 09hh24mm38.9ss, +56dd07mm46ss respectively. The source is chosen for two reasons:

- it is bright enough with B-mag of 17.60
- its redshift is 0.024 which shift its $H\beta$ line just above the OIII narrow band filter available al 1.3m DFOT.

The another advantage of this source is that it is a low luminosity AGN with $L_{5100} = 0.011409258 \times 10^{44}$ erg/s. Based on the commonly used radius luminosity relation available in Bentz et al. (2009), its typical R_{BLR} is found to be around 3.1 light days. As a result, monitoring of this source for about two weeks time can in principle enable us to estimate R_{BLR} precisely using PRM. The observation for this was carried out during 14 December 2016 to 3rd of January 2017 for 11 epochs in V, B and OIII bands using 1.3 m DFOT. During each observation three photometric standards were also observed in Landolt field. This source is nearby low luminous AGN at a redshift of 0.024 which is an extended source rather than point like which is the case for quasars. To make the host galaxy contribution constant in each source frame, so that it does not affect the variability of AGN, we took instead of mean Full Width at Half Maximum (FWHM), the maximum value of FWHM obtained using 6 moderately bright stars of the frame excluding the source. To ensure that the galaxy contribution in all the 11 epochs of observation is same , we took for final photometry a single FWHM as maximum among the 11 epochs. This procedure is repeated for the photometry in all the three bands by computing 2nd aperture magnitudes along

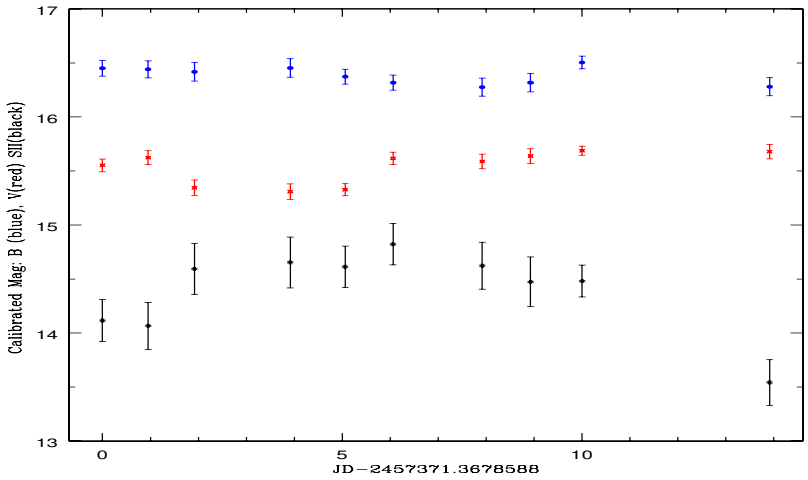

Figure 3.1: Differential Light Curves (DLCs) for our target object. Here the DLC is derived using 'non-varying' comparison stars (s2)

with its error as this aperture is found to give the highest SNR. For deriving the light curve of source, we have done both differential as well as absolute photometry.

In differential photometry, light curve for target object is drawn by taking difernce with respect to non varying comparison stars. To select the non varying comparison stars we have taken various 2 stars combinations (excluding the source) and checked them visually for the steadiness of their differential light curve (DLC). As target object and comparison stars are on the same frame, they suffer the same amount of extinction. Advantage of differential photometry is that the various instrumental effects associated with target source get removed on taking difference with these stars. If source is variable, then it shows variability w.r.t. these stars.

For absolute photometry, we applied the following procedure:

Apparent magnitudes are not extinction corrected, so we do extinction and exposure

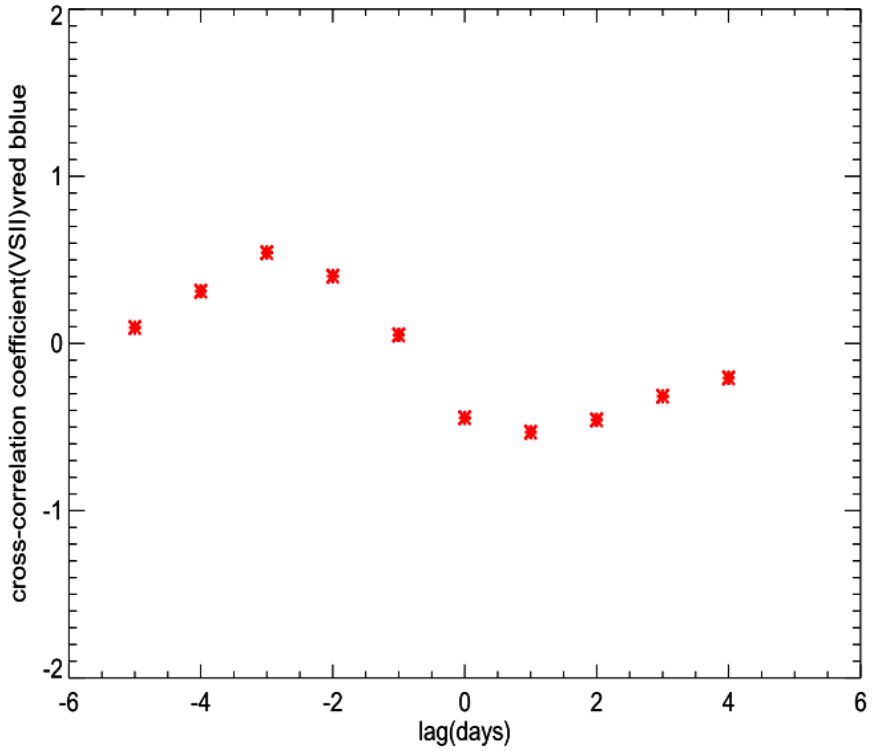

Figure 3.2: Cross-correlation coefficient(between V and SII) vs lag for calibrated mag

time correction in order to find instrumental magnitude. This is calculated by using expressions for extinction coefficients as:

$$
\begin{aligned}
\mathrm{M}_{inB} &= M_{apB} - 0.32 \times X + 2.5log(t) \\
eM_{inB} &= \sqrt{eM_{apB}^2 + (0.05 \times X)^2} \quad for \quad Bband \\
M_{inV} &= M_{apV} - 0.21 \times X + 2.5log(t) \\
eM_{inV} &= \sqrt{eM_{apV}^2 + (0.06 \times X)^2} \quad for \quad Vband \\
M_{inOIII} &= M_{apOIII} - 0.27 \times X + 2.5log(t) \\
eM_{inOIII} &= \sqrt{eM_{apOIII}^2 + (0.17 \times X)^2} \quad for \quad OIII \\
Here, X &= sec(z) = Airmass
\end{aligned}
\tag{3.1}
$$

3.1.2 Cross correlation analysis

We performed a cross correlation analysis using the ICCF method. The cross correlation was done between the flux obtained from V and OIII filters. The plot of Cross-correlation coefficient as a function of time lag is given in (Figure 3.2) between V and OIII filter, giving maximum shown in (Figure 3.2). Using above relation, we calculated lag which is 3 days. From measured time delay (τ_d), we calculated the BLR size as , R = cτ_d , hence, R=(3.00 ± 0.22) light days. Here, c=speed of light

3.1.3 Host Contribution

The spectra of low redshifted AGNs contains significant amount of stellar light contribution from host galaxy. In order to extract important properties for AGN from spectra, this stellar contribution needs to be removed. This is done by simple stellar population method (SSP). This method makes use of following equation :

$$F(\lambda) = \left[\sum_{i=1}^{39} a_i \times F_{SSP}(\delta\lambda, r_\lambda\right] * g(\lambda, \sigma_*) + F_{AGN}(\lambda, r_\lambda)$$

Here, $F_{(\lambda)}$ is observed spectrum modelled from SSP. First part of right hand side of above euation represents steller contribution of host galaxy and 2nd part represents AGN contribution. Here a_i is the amplitude of individual template, $g(\lambda, \sigma_*)$ is the Gaussian broadening function with σ_* as stellar velocity dispersion, $F_{SSP}(\delta\lambda, r_\lambda)$ is SSP template with a wavelength shift $\delta\lambda$ and reddening correction factor r_λ . $F_{AGN}(\lambda, r_\lambda)$ is contribution of AGN in the form of λ^α with reddening correction factor r_λ with α as power-law index. As the SSP consists of 39 spectral templates so summation has been applied from i=1 to 39. The templates were taken from (Bruzual & Charlot, 2003). A detailed description of the SSP method is given in (Bruzual & Charlot, 2003) and (Zhang, 2014). This method gives us decomposed contribution of host galaxy and AGN power law continuum. We then masked the emission line without considering Fe II multiplets as emission lines to leave sufficient space for continnum fitting and then fitted the spectra using IDL mpfit [1] fitting package. We then subtracted host galaxy contribution from spectra obtained after SSP method to have only AGN contribution.

3.1.4 Emission Line Fitting

After subtracting host galaxy contribution from spectra, we performed emission line fitting process around $H\beta$ and $H\alpha$ region including one local power-law continnum along with recent high- quality Fe II template spectra taken from (Kovacevic et al., 2010). The wavelength range in $H\alpha$ region is $6280 - 6750\mathring{A}$, the lines fitted for this region are narrow $[O_I\ ]\lambda 6300, 6363\mathring{A}$, narrow $[N_{II}]\lambda 6548$, $6583\mathring{A}$ doublet, and the narrow $[S_{II}]$ λ 6716, 6731 $\mathring{A}$ doublet along with H. For $H\beta$ region, the wavelength range is $4385 - 5500\mathring{A}$ contains both narrow and broad line components and the lines fitted for this regions are $HeII\lambda 4687\mathring{A}$ and $[O_{III}]$ λ 4959, 5007 $\mathring{A}$ doublet (with

[1] https://idlastro.gsfc.nasa.gov/ftp/pro/markwardt/mpfit.pro

two Gaussian functions). Each narrow line component is fitted with Gaussian distribution having maximum FWHM of 1200 km s^{-1} (see, Shen et al., 2011b). From theoretical arguments, (Goad et al., 2012) suggests that broad line components of NLSy1 galaxies have a Lorentzian profile rather than Gaussian caused by microscopic turbulence velocity of BLR clouds resulting in enhanced wings relative to the core at a large radius. Observations show that the observed broad Balmer lines are best characterized by a Lorentzian than a Gaussian profile. Therefore, for broad line component of Balmer lines, both distributions are used for fitting process where algorithm automatically chooses the best one for fitting process and gives the same width for broad line components when both $H\beta$ and$H\alpha$ regions are fitted simultaneously . During the fitting process, the flux ratios of $[O_{III}]$ and $[N_{II}]$ doublets were fixed to their theoretical values, i.e., $F(5007)/F(4959) = 3$ and $F(6585)/F(6549) = 3$. Width of all narrow components in $H\beta$ region were tied with the narrow $[O_{III}]$ line width and the redshift of each doublet was tied together (see, Shen et al., 2011b). Similarly, the width for $H\alpha$ region were tied with narrow $[N_{II}]\lambda$ 6583 $\mathring{A}$. Final fitting process is done by varying all the free parameters using least square minimization method along with Fe II templates to have emission line parameters from host galaxy subtracted spectra. Figure 3.3 shows fitted spectra of emission lines.

From spectra, knowing emission line parameters we calculated FWHM for Hβ emission line for MCG09 to be 1917.456 ± 24.316 km/s. Therefore, the black hole mass (M_{bh}) of MCG09 as from virial relation of $(FWHM)^2 = f * GM_{bh}/R$, with 'f' being a geometric correction factor (including acretion disc inclination etc.) and R distance from central engine to BLR comes out to be $\sim (2.87 \pm 0.45) \times 10^7 M_\odot$ where we assumed f=3/4 for spherical distribution, $M_\odot = 1.989 \times 10^{30} kg$ is the solar mass.

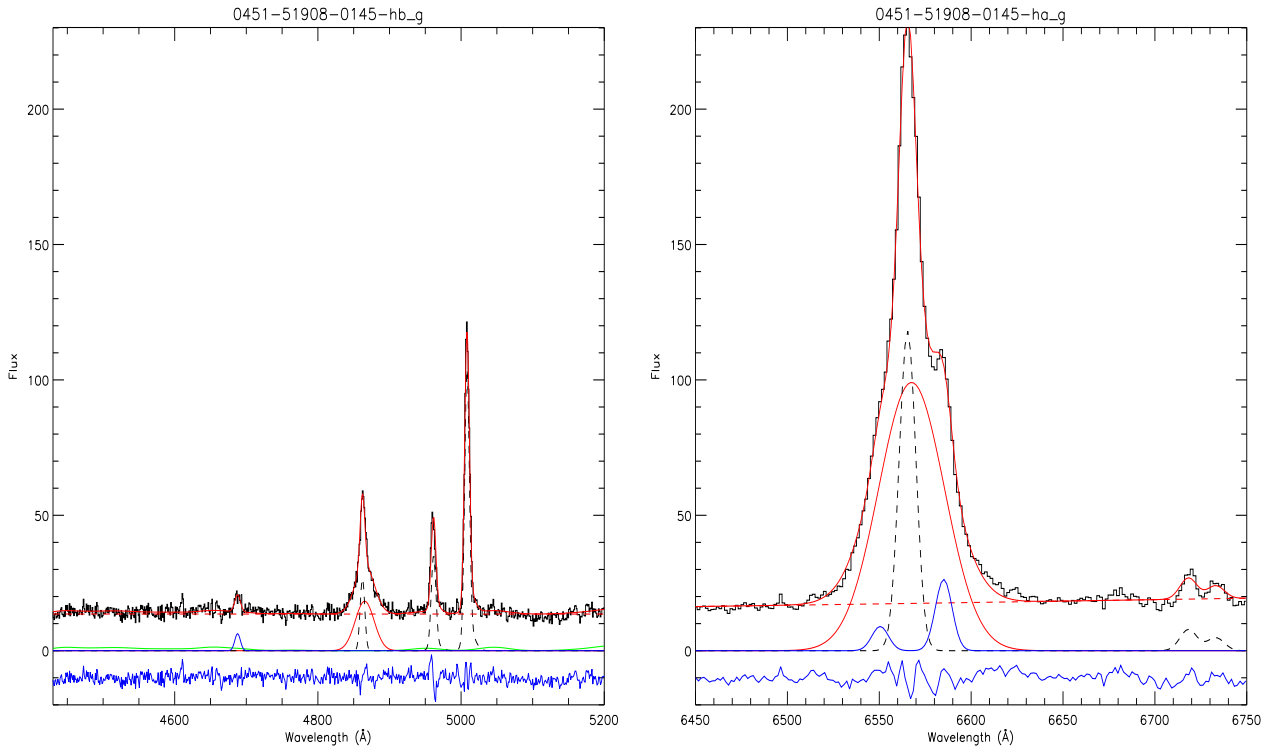

Figure 3.3: Simultaneous spectral fitting around Hβ (left) and Hα (right) emission line regions. The labels are PLATE-MJD-FIBER of SDSS. In the Hβ region (left), the observed spectrum (black) and the overall fitted spectrum (red) are shown with the decomposed individual components; broad Hβ in green, narrow components (Hβ_n, [O III] doublet) and broad He II line in blue, broad [O III] doublet in magenta, and Fe II lines in brown. In the Hα region (right), the observed spectrum (black) and the overall fitted spectrum (red) is shown with the decomposed individual components; broad Hα in red and narrow components (Hα_n, [N II], [S II] doublets) in blue.

3.1.5 Results and discussions

Using PRM technique, we obtained a time delay of (3.00 ± 0.22) days between continuum and emission line flux and hence BLR size of (3.00 ± 0.22) light days. Using spectroscopy, we calculated FWHM of Hβ emission line as $1917.456 \pm 24.316\ kms^{-1}$ means that the broad emission lines are indeed originating in the BLR region. From virial relation, we also calculated black hole mass which is $(2.87 \pm 0.45) \times 10^7 M_{\odot}$. Based on commonly used L-R relation, we calculated black hole mass which is $(2.97 \pm 0.46) \times 10^7 M_{\odot}$ and there is consistency between these two calculated black hole masses from PRM and the other from the empirical L-R relation. Since our choice of the target object detected here is according to narrow band filter available at 1.3m DFOT and this filter is not properly calibrated, also not properly tuned to redshifted $H\beta$ emission line, so there is possibility of some discrepancy in the results obtained. Also, the source selected is also not variable with high amplitude as would be needed to do proper PRM. However, the errors we get in PRM is also very small, means that the observations of such low luminous AGNs are feasible from 1.3m DFOT. In future with the arrival of more narrow band filters tuned to the redshift of Hβ and Hα emission lines, we may get precise BLR sizes and SMBH mass estimates.

3.2 Calibration of photometric reverberation mapping with spectroscopic reverberation mapping

In this project, we obtained a data set for which the reverberation lags were calculated using the spectroscopic techniques. We convolved the spectra with the transmission curves of our filters to get the photometric data points. The photometric data points

generated were treated as if they were indeed taken using the narrow band filters. We then compared the results of the two methods.

3.2.1 Data

We obtained data from the LICK AGN monitoring project (LAMP) 2008 [2] in the form of multi epoch spectra (see Table 3.1). Details about the dataset is available in Walsh et al. (2009). The project consisted of mostly continuous 64-night spectroscopic monitoring campaign at the Lick Observatory 3m Shane telescope, along with simultaneous nightly B and V imaging carried out at four smaller telescopes: the 0.76m robotic Katzman Automatic Imaging Telescope (KAIT), the 2m Multicolor Active Galactic Nuclei Monitoring telescope (MAGNUM), the Palomar 60 inch telescope (P60), and the 0.8m Tenagra II telescope. It was a reverberation-mapping campaign that targeted 12 low redshifted ($0.005 < z < 0.044$), low luminous Seyfert 1 galaxies containing black holes with expected masses between $10^6$and $10^7 M_\odot$ and $H\beta$ reverberation lags between 5-20 days and also the well-studied AGN NGC 5548 with a black hole mass of $6.54 \times 10^7 M_\odot$. Most of the previous reverberation campaigns measured the AGN continuum variations directly from the spectra. However, for this sample of relatively low-luminosity AGNs, measuring the continuum flux from broadband image seemed more accurate, as a better calibration and a higher signal-to-noise ratio (S/N) was obtained using images rather than spectra. Lags for 9 sources out of a total of 13 were obtained in Bentz et al. (2009) since they could not get good correlation for rest 4 of the sources. We obtained spectra for these sources and extracted the $H\beta$ emission line light curves using spectral decomposition and the continuum light curves were obtained from the observations in the B and V band. The light curves for these bands are in terms of Vega magnitudes, which needed to be converted into flux units for our analysis.

[2] https://www.physics.uci.edu/~barth/lamp.html

Table 3.1: **The sample of AGN selected for this analysis from LAMP Dataset.**

S No. .	Name	RA (J2000) (hh mm ss)	Dec (J2000) (deg mm ss)	Redshift (z)	$\sigma_{H\beta}$ (km/sec)
1	Mrk 142	10 25 31.3	+51 40 35	0.04494	1183.24
2	SBS 1116+583A	11 18 57.7	+58 03 24	0.02787	4405.94
3	Arp 151	11 25 36.2	+54 22 57	0.02109	2098.24
4	Mrk 1310	12 01 14.3	-03 40 41	0.01941	2903.30
5	Mrk 202	12 17 55.0	+58 39 35	0.02102	7171.31
6	NGC 4253	12 18 26.5	+29 48 46	0.01293	1207.91
7	NGC 4748	12 52 12.4	-13 24 53	0.01463	1181.71
8	NGC 5548	14 17 59.5	+25 08 12	0.01718	4746.46
9	NGC 6814	19 42 40.6	-10 19 25	0.00521	2289.15

3.2.2 Spectroscopic lags

We explored the methods of lag estimation and found out that JAVELIN is at par if not better than traditional CCF methods in a previous study. In the literature, (Zu et al., 2011; Grier et al., 2018; Mudd et al., 2018) etc. have concluded the same with their datasets. Keeeping this in mind, we used this method exclusively during this work. JAVELIN[3] is a Markov Chain Monte Carlo (MCMC) based code developed by Zu et al. (2011). It first models the variability of the AGN as a Damped Random Walk (DRW) or in other terms an Ornstein Uhlenbeck (OU) process for timescales longer than a few days. This approach has been demonstrated by Kelly et al. (2009) and MacLeod et al. (2010) where they applied the same model to a large number of quasar light curves. The covariance function for this DRW process takes the following form:

$$S(\triangle t) = \sigma_d^2 e^{(-|\triangle t/\tau_d|)} \tag{3.2}$$

[3] https://bitbucket.org/nye17/javelin

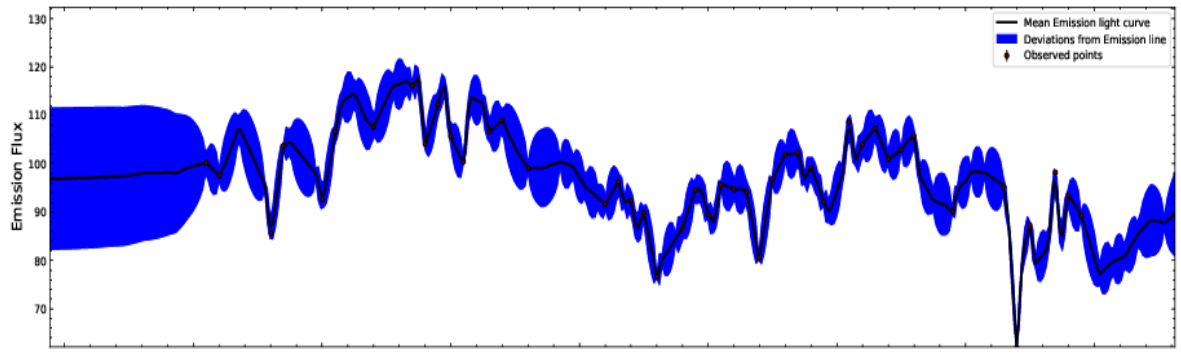

(a) Emission line light curve as obtained from JAVELIN

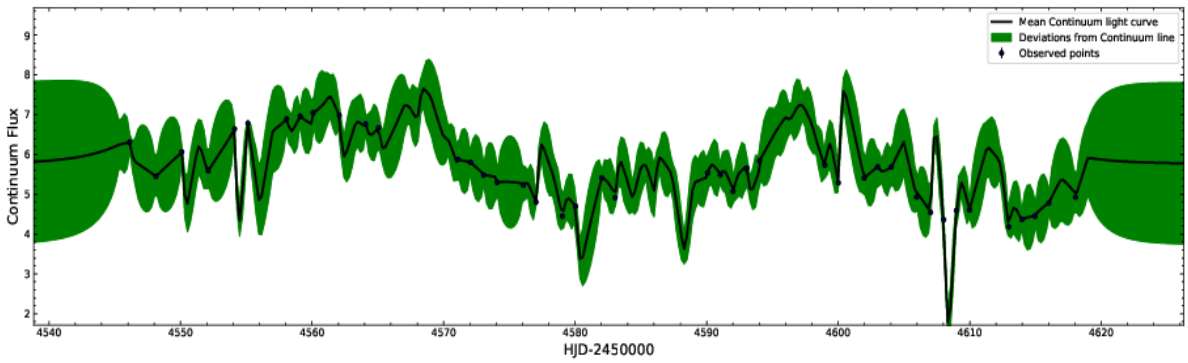

(b) Continuum light curve modelled as a damped random walk (DRW) obtained through JAVELIN.

Figure 3.4: The continuum and the emission line light curves as obtained from JAVELIN. It first models the variability as a random walk process and then builds the emission line light curve by shifting, scaling and smoothing the continuum light curve and builds a probability distribution for various parameters including the lag. [The flux units are $10^{-15} erg.s^{-1}.cm^{-2}$.]

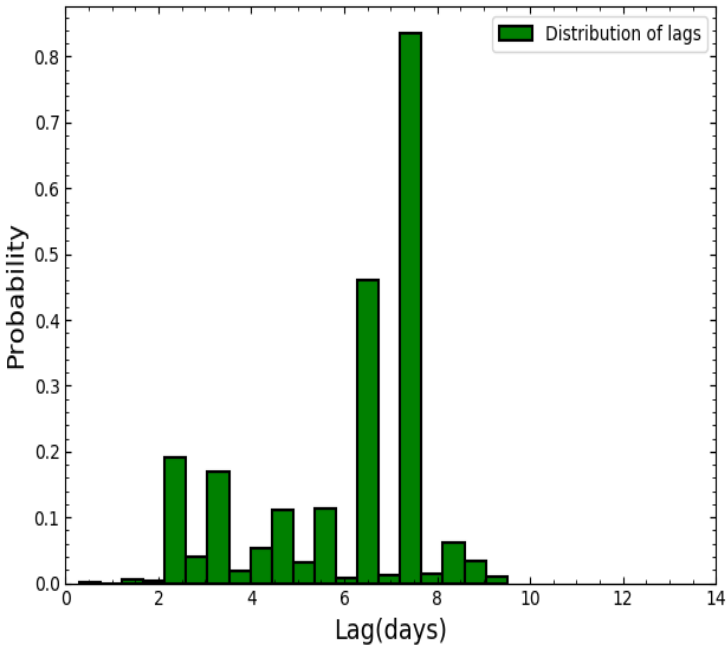

Figure 3.5: The probability distribution for the lag as obtained through JAVELIN for NGC 6814.

where $\triangle t$ is the time interval between the two epochs and σ_d and τ_d are the amplitude and the time scale of variability respectively. Only these two parameters play a role in the variability of the quasar. Lag estimation in JAVELIN is based on the the ansatz that emission line variability is a scaled, smoothed and displaced version of the continuum. Initially, it builds a continuum model to determine the DRW parameters σ_d and τ_d of the continuum light curve. Then JAVELIN assumes that the emission line lightcurve, is a shifted, smoothed and scaled version of the first lightcurve (see Figure 3.4). This fits three additional parameters for emission lines: the time lag, the top hat smoothing factor and the flux scaling factor (Yu et al., 2018). The time lag between the two light curves is obtained in the form of a distribution with the peak showing the maximum probability (see Figure 3.5).

The data was obtained in the form of spectra as well as B and V band light curves. We converted the B and V light curves from the units of magnitudes to that of flux as flux varies linearly, while the magnitudes vary in log scales. The emission line light

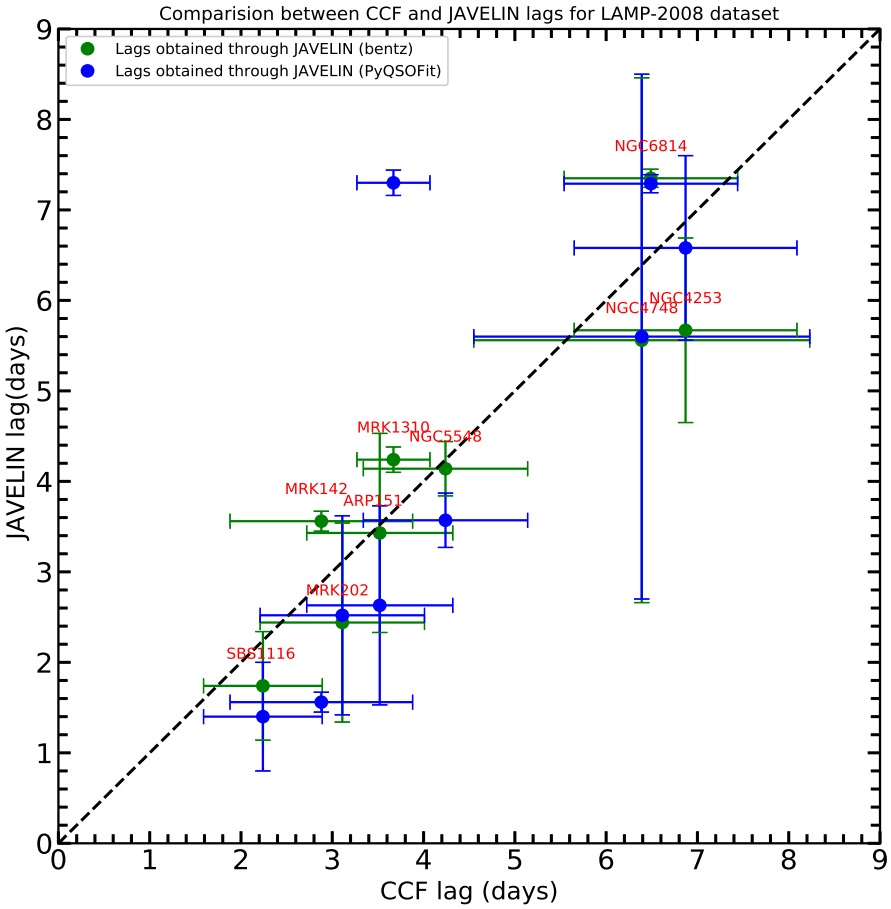

Figure 3.6: Comparision between lags obtained using JAVELIN and that obtained using ICCF method. The blue dots are obtained from th $H\beta$ light curves prepared by us using spectral decomposition while the green dots are from the light curves available in Bentz et al. (2009).

curve was prepared from the spectra. The spectral decomposition was performed using a recently developed code[4] : PyQSOFit (Guo et al., 2018). It simultaneously fits the emission lines as single or multiple gaussians, continuum as a power law, and also fits the iron blends using given optical/UV templates. The host galaxy contribution is removed for a defined redshift range based on the galaxy tempelates. We obtain the fit for$H\beta$ emission profiles, estimate the area under the curve and find the FWHM of the emission line. The flux is obtained by integrating over the line limits. We prepare the $H\beta$ line light curves by repeating the process for the spectrum at every epoch for each source and estimate the reverberation lags between the $H\beta$ line and the B and V band continuum. All the lag estimates are in the observers frame and the actual values will be reduced due to time dilation effects. We compared the lags obtained using our methods, with the ones available in Bentz et al. (2009) and found good correlation between the two (see Figure 3.6). For example, we obtained a BLR size of $3.43^{+1.11}_{-0.13}$ light days for ARP151, $7.35^{+0.10}_{-0.08}$ light days for NGC6814, $1.74^{+0.66}_{-0.34}$ light days for SBS1116+583A and $4.14^{+0.31}_{-0.53}$ for NGC5548, while published values (in above paper) for the same sources are $3.52^{+0.82}_{-0.72}$, $6.49^{+0.95}_{-0.96}$, $2.24^{+0.65}_{-0.61}$ and $4.24^{+0.1}_{-1.35}$ light days respectively. This way we re-establish JAVELIN as a suitable method for lag estimation.

3.2.3 Photometric lags

In order to understand the complications involved with the Photometric Reverberation mapping technique, we need narrow and broad band photometric light curves. As we have the transmission curves of the narrow band filters available, the photometric lightcurves were prepared by convolving the transfer function of filters with the $H\beta$ emission line, to get the flux as it would be obtained if we observe through these filters. A simliar approach has been adopted by Zhang et al. (2017b) as well.

[4] https://github.com/legolason/PyQSOFit

Now, the first complication arising out of this method is that the underlying continuum cannot be removed from the emission line flux. This is a problem related with PRM and Haas et al. (2011) overcame it by subtracting the the scaled V band light curve from the narrow band $H\beta$ line light curve. (Edri et al., 2012) undertook observations in SDSS g', r' and i' bands. This way, the i' band consisted of the continuum flux only while the g' and r' bands consisted the continuum as well as $H\beta$ and $H\alpha$ flux respectively. Later, they subtracted the i' band flux to get pure $H\beta$ and $H\alpha$ line flux. We first check how much the lag values deviate from their spectroscopic counterparts to get an idea of the role of continuum flux in the deviations. The lags were obtained, and there was a significant deviation indeed (see Figure 3.7). For 4 out of 9 sources the lag deviations were within 1 day, which can be tolerated as an error, but for NGC 6814 the photometric light curve yielded a lag of $1.36^{+0.13}_{-0.82}$ days and if compared to spectroscopic lag of $7.35^{+0.10}_{-0.08}$ days, the deviation is enormous. We suspected the strength of the emission line could impact the extraction of lags, thus obtained the mean equivalent width of $H\beta$ line for each source and saw the variation of deviation with respect to the equivalent width. It turned out to be random, which leads us to think that the line strength doesn't have a role to play in the estimation of reverberation lags, although we refrain from making any conclusions based on this result.

We look for possible solutions to overcome this deviation. A possible solution is to observe in a band with no significant emission lines, most probably the I band which would trace only the continuum flux as done by Edri et al. (2012). Later we can subtract this continuum level from the source to obtain the lags. To check how continuum subtraction would help, we again convolved the transfer function of the filters with the continuum level both blue and red side of the emission line. This way we obtained the continuum flux and after averaging the two, subtracted the flux from the $H\beta$ emission line. Thus, we obtained continuum free $H\beta$ flux. Through this

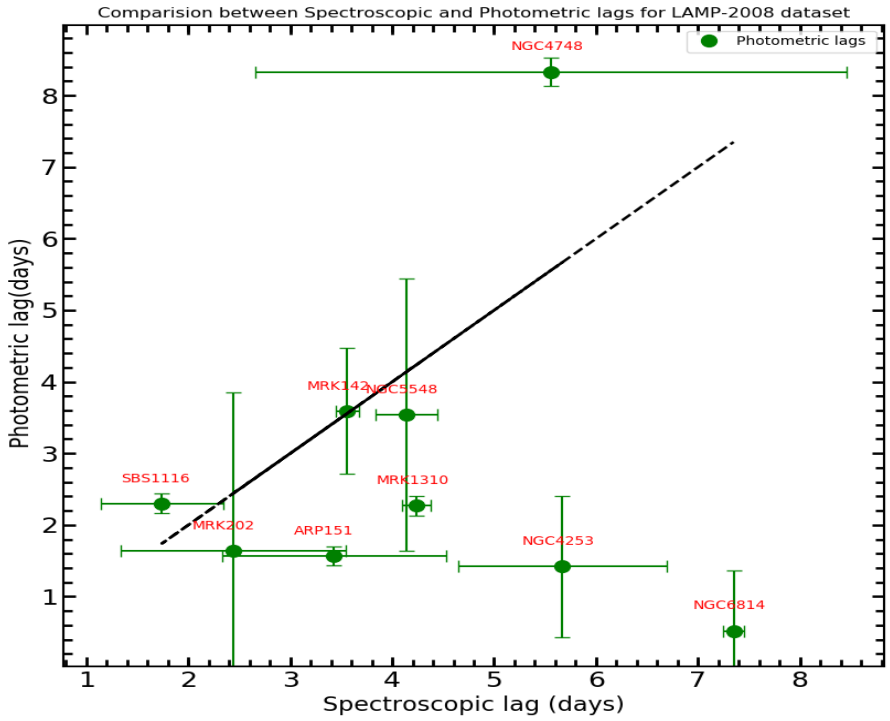

Figure 3.7: Comparision between spectroscopic and photometric lags obtained using JAVELIN. There is a significant deviation if pure emission line flux is not used for lag estimation.

Table 3.2: **A comparision of reverberation lags for $H\beta$ line obtained in this work alongwith the BH mass estimated through the spectra. (All lag estimates are in light days and M_{BH} are in units of $10^6 M_\odot$).**

S No.	Name	Lag Bentz et al. (2009)	Spectroscopic Lag	Photometric Lag	Continuum removed Lag	M_{BH}
1	Mrk142	$2.88^{+1.00}_{-1.01}$	$3.56^{+0.11}_{-1.03}$	$3.58^{+0.88}_{-1.06}$	$4.48^{+0.97}_{-0.90}$	$6.74^{+1.46}_{-1.35}$
2	SBS1116	$2.24^{+0.65}_{-0.61}$	$1.74^{+0.66}_{-0.34}$	$2.33^{+0.11}_{-0.84}$	$3.46^{+4.11}_{-0.86}$	$72.2^{+8.5}_{-17.9}$
3	Arp 151	$3.52^{+0.82}_{-0.72}$	$3.43^{+1.11}_{-0.13}$	$7.49^{+0.13}_{-2.90}$	$4.68^{+0.61}_{-1.09}$	$22.16^{+2.88}_{-5.16}$
4	Mrk 1310	$3.67^{+0.46}_{-0.50}$	$4.24^{+0.14}_{-0.68}$	$2.27^{+0.11}_{-0.78}$	$2.39^{+0.97}_{-0.96}$	$21.67^{+8.79}_{-8.7}$
5	Mrk 202	$3.11^{+0.91}_{-1.12}$	$2.44^{+1.10}_{-0.93}$	$1.61^{+0.87}_{-0.10}$	$3.47^{+1.05}_{-0.98}$	$191.90^{+58.09}_{-54.22}$
6	NGC 4253	$6.87^{+1.22}_{-1.84}$	$5.67^{+1.02}_{-0.19}$	$1.42^{+0.99}_{-1.01}$	$4.72^{+0.83}_{-0.18}$	$7.39^{+1.30}_{-0.28}$
7	NGC 4748	$6.39^{+1.84}_{-1.46}$	$5.56^{+2.90}_{-0.95}$	$8.33^{+0.16}_{-0.19}$	$8.54^{+0.96}_{-0.15}$	$12.81^{+1.44}_{-0.22}$
8	NGC 5548	$4.24^{+0.91}_{-1.35}$	$4.14^{+0.31}_{-0.53}$	$3.54^{+1.93}_{-0.07}$	$4.57^{+1.00}_{-0.13}$	$110.76^{+24.23}_{-3.15}$
9	NGC 6814	$6.49^{+0.95}_{-0.96}$	$7.35^{+0.10}_{-0.08}$	$1.36^{+0.13}_{-0.82}$	$7.36^{+0.10}_{-0.80}$	$41.49^{+0.56}_{-4.51}$

technique, deviation in lag values reduced significantly. For example, for the same source NGC 6814, the new lag estimate is $7.36^{+0.10}_{-0.80}$ days which means, the technique worked perfectly for this source. We estimated lags for all the sources and thus, we can conclude that this technique is promising. In real world, it would be extremely difficult to monitor a source in a fashion described above. Thus, although promising the technique will not be practical. We are working on a few other methods as well so as to choose the best way to remove continuum flux. Another problem with photometric monitoring is the host galaxy contribution to to flux. If spectroscopic method is used, the galaxy contamination can be removed using spectral decomposition techniques, which is not possible in photometric monitoring. A few methods are available such as the Flux Variation Gradient (FVG) method which utilizes the UV to optical color ratio of the total AGN flux (Ramolla et al., 2015).

3.2.4 Results and Conclusion

Through this project, we estimated the BLR size and the Black hole masses for AGN in the LAMP 2008 dataset. We used MCMC based code JAVELIN for our analysis which is different from the traditional ICCF method used originally on the dataset. The spectra were decomposed into individual components using PyQSOFit and the emission line light curves were prepared by integrating within the line limits. The spectroscopic lags were in agreement with the lags available in literature. We convolved the spectra with the transfer function of our narrow band filters to convert spectra into photometric light curve and there were huge deviations in the lag estimates. We tried to overcome these deviations by measuring the continuum flux alongside the $H\beta$ emission line and subtracting it and through this technique, deviations in the recovered lags were reduced significantly. The question was that if there is any systematic offset, or only loss of accuracy while using photometric data instead of spectroscopic data. The answer to this question would be, if the continuum flux is removed, the photometric data yields lags at par with spectroscopic data. We performed correlation between the two emission light curves, to check if some systematic error was involved with the production of light curves itself, but the correlation peaked at zero lag meaning there was no such error.

Since PRM is a technique that can still be said to be in development stages, the aim of this project was to raise questions regarding the complications involved with PRM and we have been successful in addressing a few of them. The first would be, since the continuum can't be removed from the emission line if observed through narrow band filters, how would we take care of that? As evident through Figure 3.7, it can cause huge deviations in lag estimates.We also need to understand how this deviation plays a role in BH mass esimate. Another problem is the contribution of host galaxy which can't be removed normally. The FVG method mentioned above

looks promising and we have started working on simulations regarding it by varying the host galaxy contribution fraction and estimating reverberation lags. Since, we are targeting low luminosty AGN at low redshift, and based on RL relation, the lags for such sources should be in the range of 5-15 days, another question we are seeking answer to, is how sampling would affects the lag estimates. We hope to answer these questions in the upcoming days.

3.3 Photometric Reverberation mapping of J115138.1+561331.8

3.3.1 Photometric monitoring

In the recent observing cycle, the AGN J115138.1+561331.8 having spectroscopic redshift (z) = 0.0509 was monitored on 12 epochs between 16 May 2020 and 2 June 2020, with the 1.3m Devasthal Fast Optical Telescope (DFOT). The standard field 'SA104' was also observed for calibration during the photometric campaign. Broad-band continuum emission was measured in B and V filters. The redshift of the observed source is such that its Hβ emission line falls right on the central wavelength of one of the newly purchased narrow-band filters, i.e. the 512nm filter. This way the Hβ flux could be observed. In order to subtract the underlying continuum flux picked in the 512 nm fliter, flux measurements were also taken using the 532 nm filter, to serve as a proxy for the underlying continuum in the 512nm filter based on the results from our previous project.

3.3.2 Data Reduction

The pre-processing of the raw images (bias subtraction, flat-fielding, cosmic ray removal and trimming) was done using the standard tasks available in the Image

Reduction and Analysis Facility (IRAF). The instrumental magnitudes of the observed source and their chosen comparison stars (non varying) in the CCD frames were determined by aperture photometry (Stetson, 1987), using the Dominion Astronomical Observatory Photometry II (DAOPHOT II algorithm). Our targets are nearby low-luminosity AGNs which appear extended rather than point-like. For the aperture photometry, we have taken the maximum value of FWHM, instead of the mean FWHM obtained using 5 moderately bright stars in the observed CCD frame excluding the target AGN. This was done in order to make the host galaxy contribution constant in each science frame, so as to minimise its contribution to any genuine variability of the AGN. To ensure the same amount of host galaxy contribution for all the epochs of observation, we finally adopted the aperture radius (9.67 pixels for V-band) equal to the maximum FWHM recorded among the various observed epochs devoted to that AGN. In aperture photometry, multiple apertures which are integral multiples of the FWHM (starting from 1) are set around the target object and the magnitudes corresponding to those apertures are measured. Out of these measured magnitudes corresponding to the selected apertures (generally, 4 apertures are taken), we have adopted the magnitude corresponding to the second aperture, as this is found to give the highest SNR. Finally, this procedure is repeated for all the observed AGN for computing the second aperture magnitudes along with its error .

3.3.3 Data Analysis

Instrumental magnitude (ins) and standard magnitude (std) of standard stars are used together to find the transformation coefficients in order to standardise the target AGN. To find the transformation coefficients, we did straight line fitting by making use of the instrumental and standard magnitude of standard stars for different bands. Equations are

$$B_{std} = B_{ins} + p_B(B_{ins} - V_{ins}) + Q_B \tag{3.3}$$

$$V_{std} = V_{ins} + p_V(B_{ins} - V_{ins}) + Q_V \tag{3.4}$$

$$512_{std} = 512_{ins} + p_{512}(512_{ins} - V_{ins}) + Q_{512} \tag{3.5}$$

Here, p_B, Q_B, p_V, Q_V, p_{512} and Q_{512} are transformation coefficients. Landolt equatorial standards do not have standard magnitude in 512nm and 532nm narrow bands. Therefore, to get approximate standard magnitude in the aforementioned narrow bands, we used cubic spline fitting with U,B,V,R,I standard magnitudes (with their corresponding effective wavelength) at wavelength of H_β emission line. And finally, standard magnitudes for target source were obtained by using the above transformation equations.

3.3.4 Cross correlation analysis

We computed the cross-correlation function (CCF), taking τ values in the range from -11 to $+11$ days, in increments of 1 day. The time lag for the emission line (512nm) intensity w.r.t. the continuum (B,V) was then determined from the centroid of the CCF at amplitudes above 80% of the peak value, defined as τ_{cen}. Repeated Monte Carlo iterations were used to obtain the cross-correlation peak distribution (CCPD). We note that the time lag estimates have large uncertainties, primarily owing to the small number of the observational points available.

3.3.5 Spectral Analysis

To carefully analyze the spectra and accurately estimate the emission line parameters, we have performed a two-step fitting process (see also, Zhang, 2014) after shifting the spectra to the rest-frame.

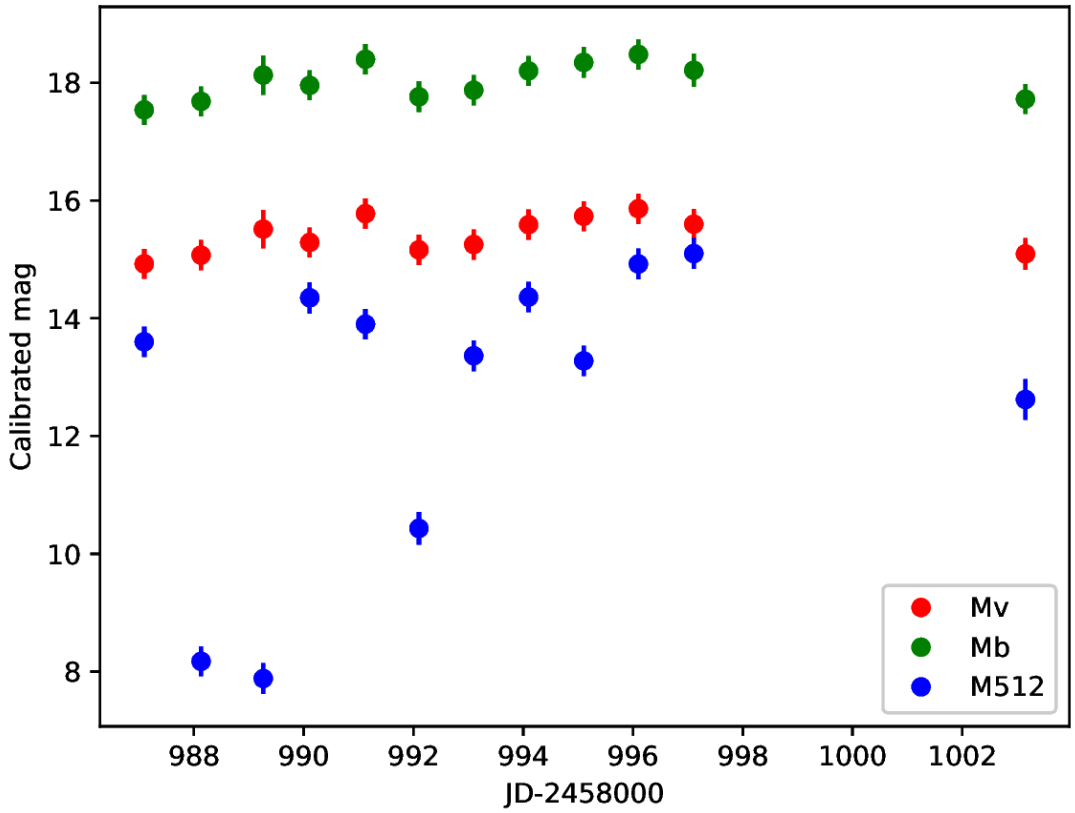

Figure 3.8: Calibrated light curves (LCs) for the observed PRM target AGN J115138.1+561331.8. We have not included the light curve for the 532 nm filter, due to the uncertain transformation coefficients obtained during the standardisation procedure.

1. The spectra were simultaneously fitted with an AGN power-law continuum (global) and stellar contribution of the host galaxy. During this step, we masked the AGN emission lines except the Fe II multiplets. We then subtracted the stellar contribution from the spectra without subtracting the AGN global continuum, and then proceeded to the next step described below.

2. In this next step, we simultaneously fitted the AGN emission lines, including the local AGN continuum, along with the Fe II template, to the host galaxy subtracted spectra obtained in the step (i) mentioned above. From this fitting, we were able to estimate the AGN's various emission-line and continuum parameters.

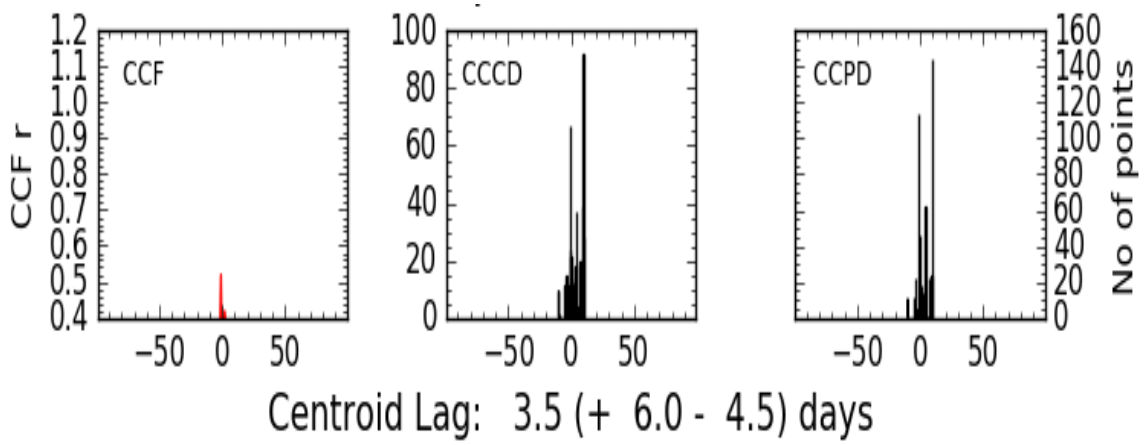

Figure 3.9: Time lag for J1151p5613 (Broadband V vs 512nm)

3.3.6 Photometric monitoring of another 2 AGN

In the recent cycle, we monitored 2 sources 1H 0323+342 and J104842.45+413302.3 for 9 and 10 days respectively with a maximum time sampling of 4 or 5 days using 1.3m Devasthal fast optical telescope (DFOT). Continuum flux were measured in broadband filters B and V. The redshift of these two sources are such that their H-α emission line falls on the one of the newly purchased narrow band filters i.e. 702nm. So, emission line flux were measured using 702nm filter.

3.3.7 Results and Discussion

Using the ICCF analysis between the broad-band V and narrow-band (512nm) light curves of the AGN J115138.1+561331.8, we have estimated a time lag of ($3.50^{+6.0}_{-4.5}$) days between its continnum and emission-line variations, yielding a BLR size of ($3.50^{+6.0}_{-4.5}$) light days. The V-band light curve has been used here for time lag estimation, in view of its closer proximity to the UV continuum of the accretion disk of the SMBH. Using the emission-line parameters determined from the available

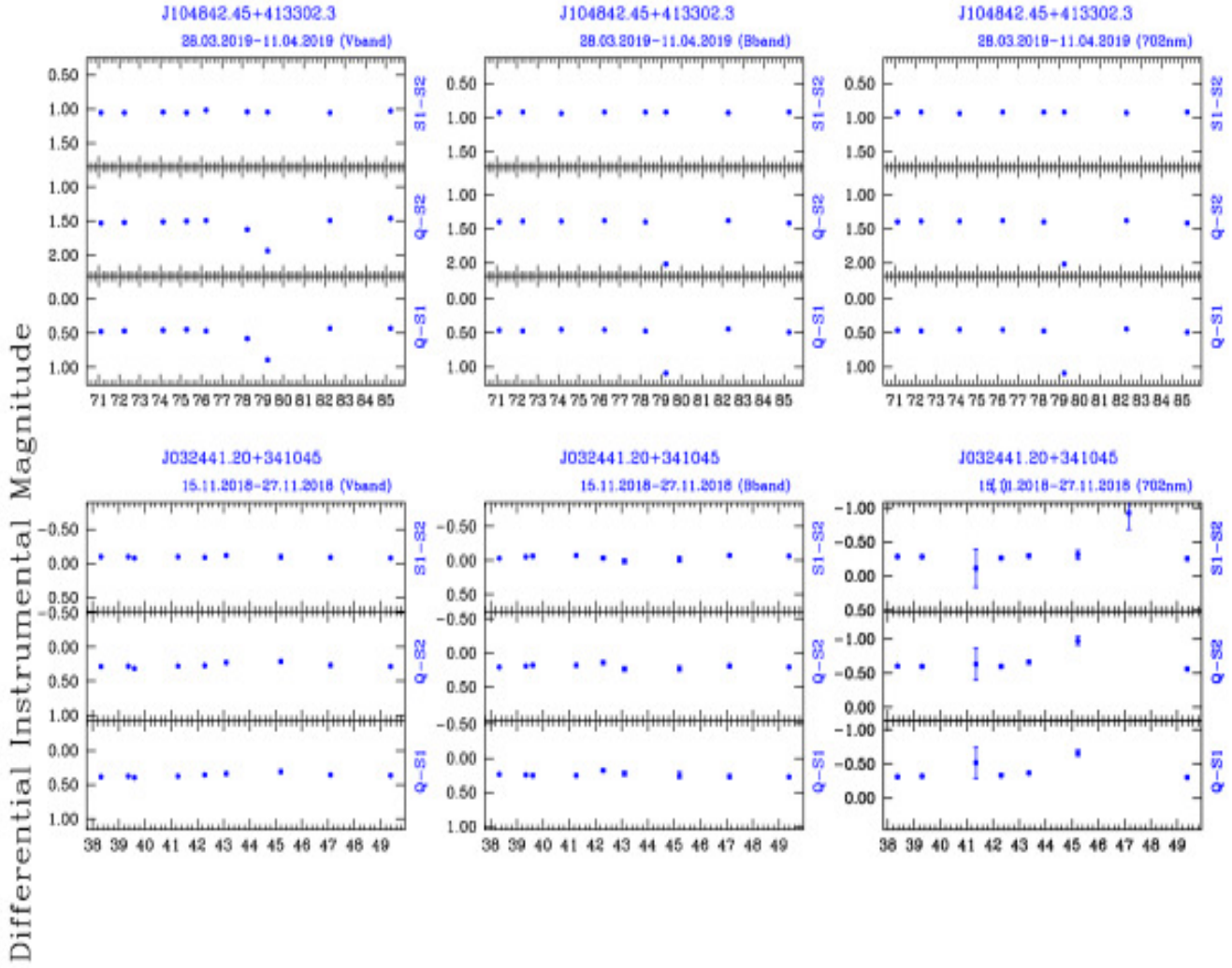

Figure 3.10: Differential light curves (DLCs) for the observed PRM sources in our sample. The first three light curves are of J1048+42.45 and the next 3 light curves are of 1H 0323+342. The name of the source, the date of observations, filter are given at the top of each light curve. The upper panel of each light curve gives the comparison star-star DLC, the subsequent lower panels give the source-star DLCs.

spactra, such as $\delta\lambda$, λ for H_{4861B} (H_{4861B} is the broad component under the black hole's gravitational influence, $\delta\lambda$ and λ are the width and centroid of the fitted line profile, respectively), we have estimated the FWHM of the emission line to be (1054.75 ± 41.53) km s^{-1} and a black hole mass of $(7.82 \pm 5.4) \times 10^6 M_\odot$ by applying the Virial relation.

By visual inspection, source 1H 0323+342 did not show any variability trend between emission light curves and broadband light curves. On cross-correlation between broad band light curve (B,V) and emission light curve (702nm), we got a time lag of 2 days for B,702nm and 1 day for V,702nm. For estimation of black hole mass, one needs velocity width of observed emission line as well. But due to the absence of optical spectra in SDSS and NED, we could not determine the velocity width of H-α emission line. As we need single epoch spectra for balck-hole mass estimation, we will use 3.6m telescope for spectra in future. Recent RM studies of this source has shown time lag of 14.85 days, but our result is very much different from this. So we are working on this aspect as well. Source J104842.45+413302.3 has a flux drop in broadband (B,V) and narrow band (702nm) light curves. But this flux drop is at the same epoch for B.V and 702 filters and according to the principle of RM, emission line lags behind continuum by some time delay. On cross-correlating broadband and narrowband light curves, we got a time delay of zero days as expected from visual inspection of differential light curves. The differential magnitude estimation corresponding to dip may be due to bad observing conditions as it was observed on a bright night.

3.4 Accretion disk reverberation mapping of AGN using ZTF data

Matter flowing onto the black hole forms an accretion disk which radiates on account of viscous heating. The thermal structure of the disk is the X-ray coming from the inner most regions and the corona, the UV coming from further outwards followed by the optical and IR continuum emissions. The Shakura Sunyaev disk (Shakura & Sunyaev, 1973) model predicts a disk size scaling with the temperature of 4/3. This model predicts a disk size based on two observable parameters, the SMBH mass and the mass accretion rate. There has been a debate whether the AGN accretion disks follow the standard SS disk model or not. Recent observations have yielded disk scaling but at an order of upto 3 times than the usual (Fausnaugh et al., 2017a; Starkey et al., 2016, etc.).

We are left with either microlensing or the continuum reverberation mapping in order to probe the size of these accretion disk. Reverberation mapping is a tool which measures the lag between the emission coming from two different regions. In the traditional method, the continuum from the accretion disk energizes the BLR clouds and the lags are estimated between the Hβ emission line and the continuum light curves. A variation of reverberation mapping employs either narrow or broad band filters to estimate the BLR size. It can be done with continuum flux as well, to estimate the inter band lags.

If these regions are observed,in multi wavelength, the longer wavelengths should lag the smaller wavelengths if the photons from the inner regions are reprocessed. The correlated signals will yield the lags as black body peaking at the corresponding wavelengths. The AGN-STORM project (Fausnaugh et al., 2017a) has provided the best dataset for reverberation mapping so far. This experiment monitored the Seyfert 1 galaxy: NGC5548 using multi band gorund and space based observations

for a period lasting around 6 months (see Figure 3.13). The conclusions from the recent accretion disk reverberation mapping camapaigns has been that the observed disk sizes are a few orders larger than the ones predicted by the Shakuyra Sunyaev models. Whether the AGN accretion disks follow the SS disk model or not has been a very important question.

3.4.1 Data

We obtained the sample of reverberation mapped quasars from various sources. The Bentz collection (Bentz & Katz, 2015) provides 62 quasars, while 44 quasars were picked up from the results available in Fausnaugh et al. (2017b). The reason for selecting this sample was that the BH masses are well constrained for this sample as compared to any other AGN. The ZTF survey telescope is a high cadence photometric monitoring project which monitors AGN in the northern sky suing a custom set of g,r and i filters. A section of the data is available for publi use. We searched for the g, r and i band light curves for a location of around 5" of the coordinates of these AGN. Almost all the AGN were observed for at least one epoch in one band. We applied a criteria of at least 15 observation epochs in each band in order to catch the disk reverberation signal. The g and r bands are well sampled in ZTF while the i band had the least no. of observations. We were left with 62 AGN after applying this criteria. The resulting analysis was done on this sample only.

3.4.2 Analysis

We estimate the lags between the obtained g,r and i band light curves for all the sources in our sample. We performed a 3 σ clipping on the light curves to exclude the points at σ deviation from the mean. Also the ZTF API provides multple light curves at a single location. We chose the OID with maximum no. of exposures,

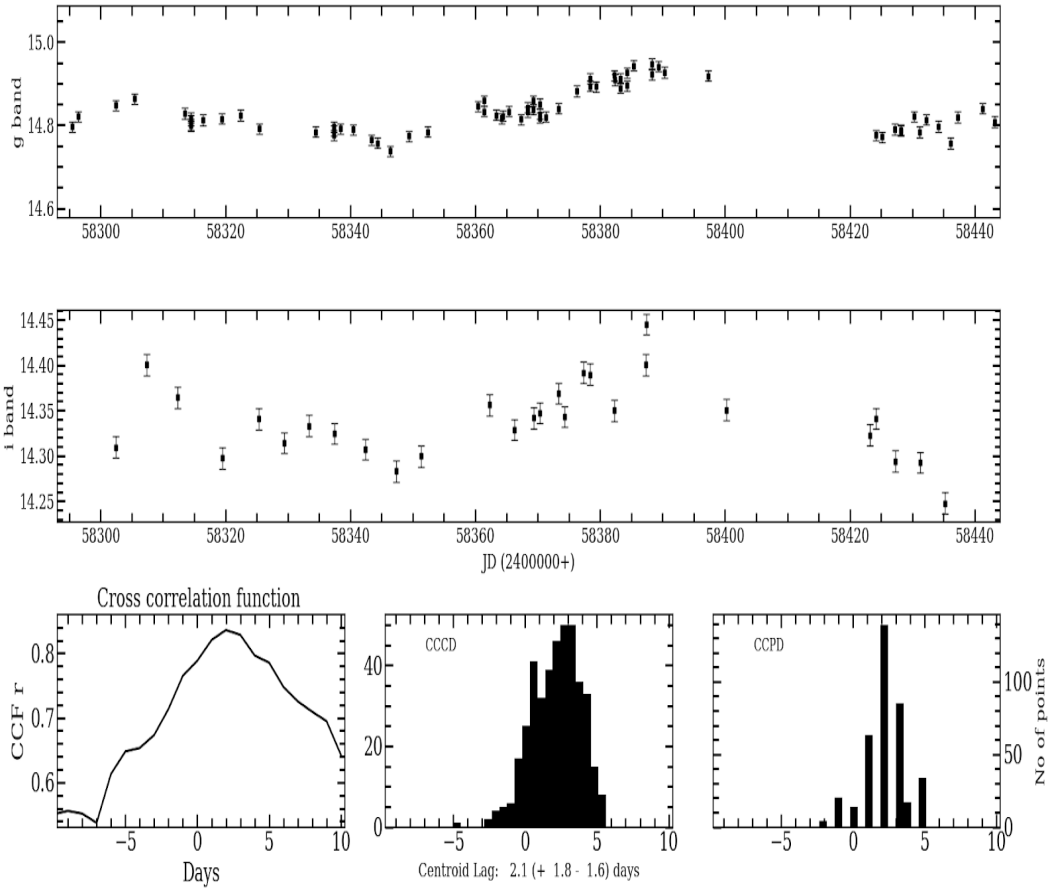

Figure 3.11: The ICCF results for MRK 335. The analysis has been run on the g and i band light curves yielding a lag of $2.1^{+1.8}_{-1.6}$ days. This lag is interpreted as the ligh travel time between the inner region radiating in g band and a slightly outer region radiating in i band.

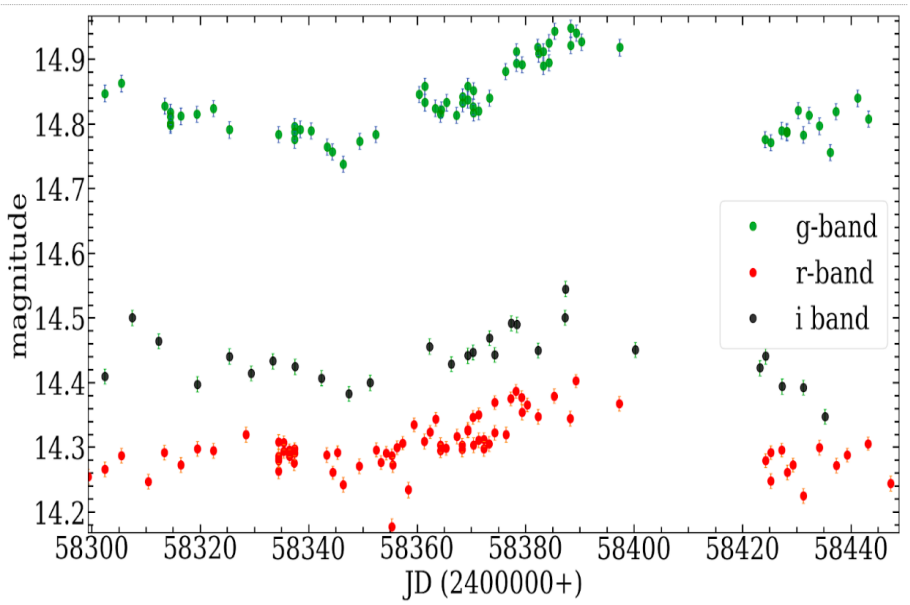

Figure 3.12: The gri band ZTF light curves for one of the sources in our reverberation mapped sample.

and the magnitudes matching with the known magnitudes in the literature or known catalogs. After preparing the light curves, we estimated the lags between the g-r and g-i filters. The expected lags for the g-r are expected to be shorter than the g-i lags. We use two different methods to estimate the reverberation lags, namely JAVELIN and ICCF.

We managed to obtain meaningful lags for only 20 of the sources from this sample. Reverberation mapping experiments face this challenge often. The light curves are not sampled properly while in some cases the variability amplitude is not sufficient to yield meaningful lags.

We put the lags in the SS disk context to understand the deviation from the standard disk model. We found out that the disk sizes obtained from the g-r ang g-i inter band lags are indeed upto an order larger than the ones predicted by the SS disk. Further analysis is going on to understand this discrepancy.

3.4.3 JAVELIN thin disk model

JAVELIN has an extension known as the *thin disk model* which attempts to directly model the accretion disk based on the light curves. The accretion disk size is given as:

$$R_\lambda = R_{\lambda_0}(\frac{\lambda}{\lambda_0})^\beta \tag{3.6}$$

here, R_{λ_0} is the disk size at λ_0 and β is 4/3=1.33 for the standard SS disk. This model gives the disk size R_{λ_0} at a given wavelength. We used the thin disk model for all the light curves. The disk size as predicted by the thin disk model vs the disk sizes as obtained from the JAVELIN and ICCF methods are not in agreement with each other. It is noticeable that the disk sizes predicted for JAVELIN assume the SS dsk as we have fixed β to 1.33 i.e. 4/3. If we compare the lags from the formula with fitted alpha, defined beta (4/3) and band wavelengths to those from the standard JAVELIN models, we are comparing what the lags are assuming a SS thin disk structure versus no assumed structure.

3.4.4 Results

The lags were recovered successfully for 20 of the sources in our sample. We obtained the lags using both the techniques: JAVELIN and ICCF. The lags for these sources match well using both the techniques even though the lags estimated through JAVELIN has lesser uncertainties. We also estimate the disk sizes using JAVELIN thin disk model which directly models the accretion disk and gives the disk size at a particular wavelength. For our sources the lag results and the thin disk model don't agree with each other, which is a discrepancy. We are understanding this discrepancy at the moment.

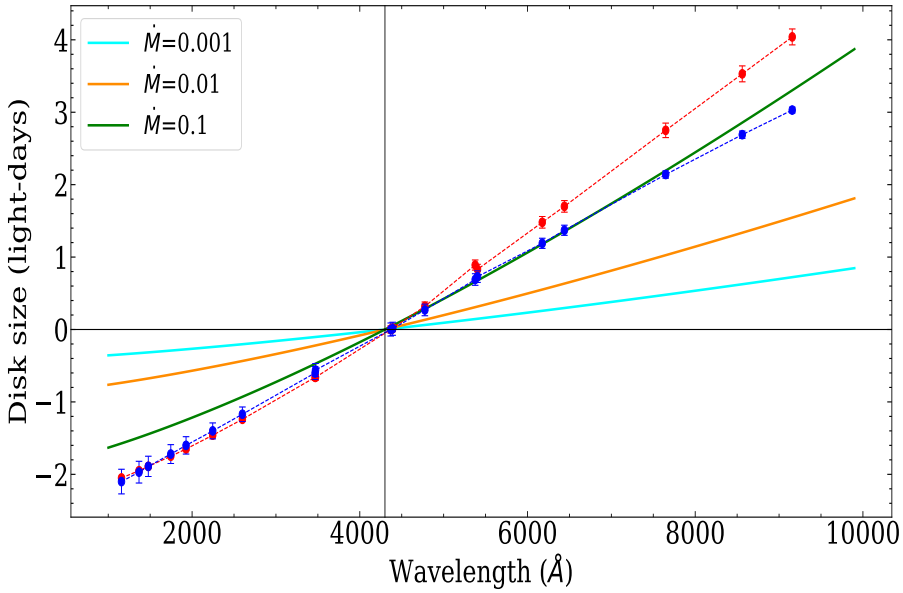

Figure 3.13: The prediction for wavelength dependent lags as predicted by the Shakura & Sunyaev (1973) disk model for various combinations of accretion rates. The blue and red lines denote the NGC 5548 lags obtained during the AGN STORM campaign using two different disk models.

3.5 Accretion disk reverberation mapping using TRT data

Resolving gas clouds of Broad Line Region (BLR) and the structure of the accretion disk in Active Galactic Nuclei (AGN) remains a formidable observational challenge even in the era of modern long baseline interferometry providing the highest possible angular resolution. Despite this challenge, resolving the size of BLR and estimation of Black Hole (BH) mass can be done thanks to the reverberation mapping (RM) technique which substitutes time resolution for the spatial resolution. The RM technique does not require a huge amount of observing time on telescopes, but requires frequent monitoring over a period of a few weeks in case of low-luminosity AGNs depending upon the size of the BLR region. Photometric reverberation mapping (PRM) allows to achieve the goals of RM even with even 1 m class telescopes by

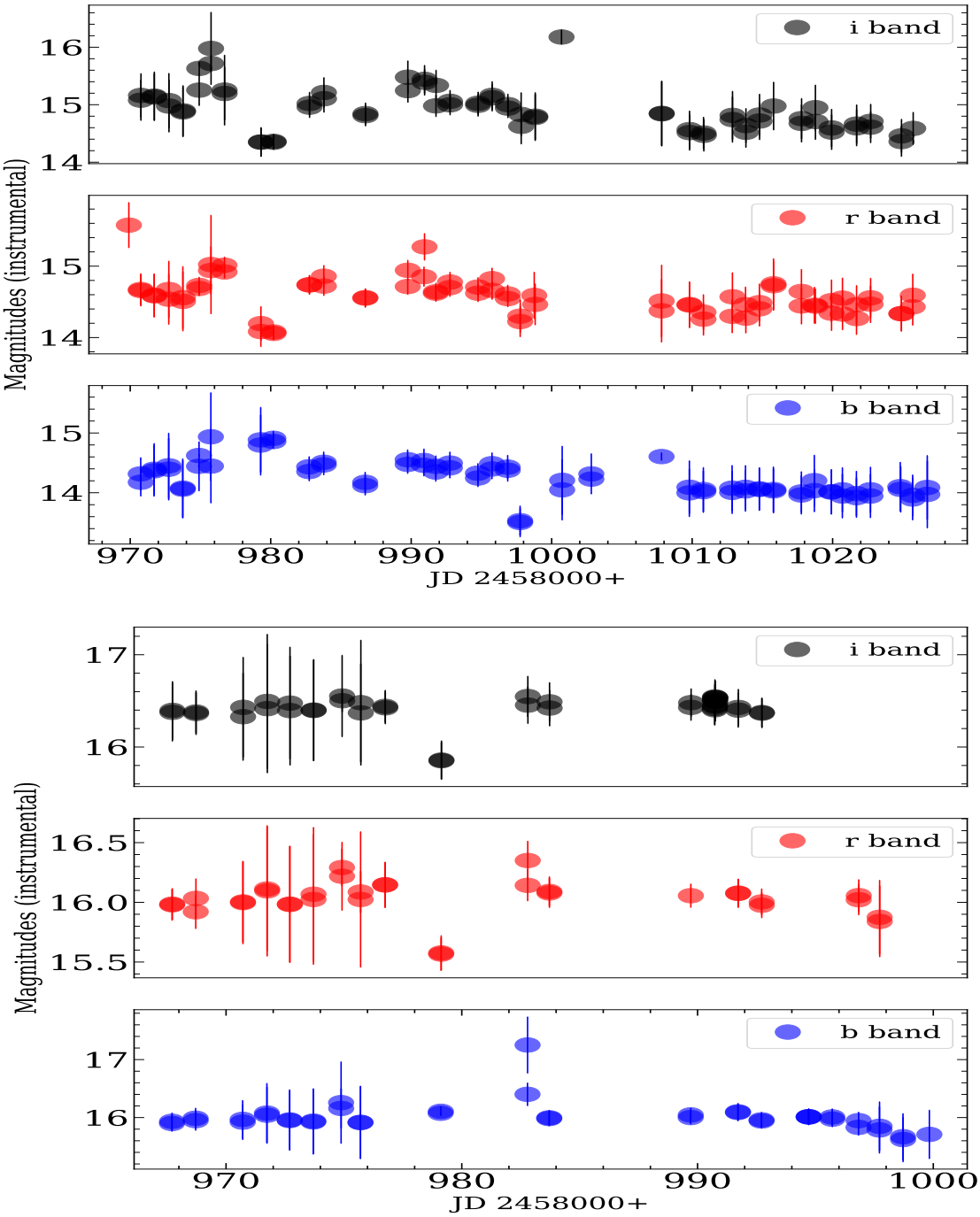

Figure 3.14: The B,R and I band light curves for NGC 5947 (top) and MCG10-16-052 (bottom) obseved using the Thai Robotic Telescopes during the months of April to July 2020.

using a combination of broad band and narrow band photometry to substitute the spectroscopic observations. While for X-ray and UV wavelength monitoring, the space based telescopes are the only feasible option, ground based broadband monitoring campaigns have proven to be important in the regard that the reprocessed UV photons are emitted in the optical wavelength range which can captured using broadband optical filters. Light curves generated with multiple band monitoring are cross-correlated with each other to obtain the lag. This lag arises due to the light travel time across the accretion disk and thus helps us estimate the size of the region at a particular wavelength.We expect meaningful reverberation lags in a monitoring campaign lasting 3 months. To get the broadband UVBRI inter band lags, we performed observations using the Thai telescopes to probe the accretion disk structure.

3.5.1 Observations

From the months of April to November 2020, we performed observation using the Thai Robotic telescopes. The aim was to get as high cadence as possible and monitor the sources for at least a couple of months. We managed to observe a set of 5 AGN: MCG 10-16-052, NGC 5947, MRK 493, NGC 6814 and MRK 509. All these AGN were monitored using VBRI filter. The reduction of the data has been done and the analysis in under progress. We aim to get the VBRI inter band lags and the interpret these lags in the context of known accretion disk models. In the ongoing cycle, we continue our monitoring of 4 more AGN to enhance our sample of accretion disk quasars.

3.6 A comparative study of BlSy1 and NlSy1 galaxies using SDSS data

3.6.1 Introduction

Seyfert galaxies are characterized by a lower luminous active nucleus as compared to the general quasar population. Among the Seyfert galaxies, Type-1 galaxies show both narrow and broad emission lines (see Netzer, 2015, for a review). These lower luminous Type-1 galaxies are subdivided into narrow and broad line Seyfert classes based on the Full Width at Half Maximum (FWHM) of the $H\beta$ emission line. NlSy1 galaxies are understood to be a subclass of active galactic nuclei (AGN) which have narrower broad Balmer line widths with FWHM of broad $H\beta$ emission line $\leq$ 2000 km/sec^{-1}, a small intensity ratio of the [O III] λ5007 to $H\beta$ line ($[OIII]/H\beta \leq 3$), stronger optical Fe II emissions (see Rakshit et al., 2017, and references therein), and usually steeper soft X-ray spectra and more rapid X-ray and sometimes optical flux variability (see Ojha et al., 2020) . It is assumed that these properties are due to the central black hole being less massive, but accreting at a very high rate. Low optical variability has also been reported in NlSy1 galaxies by Rakshit & Stalin (2017). It has been proposed by Mathur (2000) that the NlSy1 galaxies are a subcategory of BlSy1 galaxies only and can be assumed to be in evolutionary stages, while in Gaskell (2000) unusually high Fe-II strength, R_{fe} in NlSy1 galaxies is attributed to weak Balmer lines originating from a dense environment. The NlSy1 galaxies have been proposed as younger versions of the general broad line active galaxies.

The region responsible for the generation of broad emission lines is known as the Broad line Region (BLR). About 120 AGN have been studied using the reverberation mapping technique (see Bahcall et al., 1972; Blandford & McKee, 1982), which is a powerful time domain method to probe the inner regions of type 1 galaxies. However,

with the known number of AGN extending into hundreds of thousands, thanks to the all sky surveys such as the Sloan Digital Sky Survey (SDSS) (York et al., 2000) but precise knowledge of the structure and kinematics of BLR through reverberation mapping available for only a handful of AGN (see Bentz & Katz, 2015, for a comprehensive database of reverberation mapped AGN), studies have relied on statistical analysis on a selected sample of AGN constrained by various limits, to infer the physical properties. A remarkable work was done by by Boroson & Green (1992), where they performed a Principal Component Analysis (PCA) on properties derived from X-ray, optical and radio wavelength data for a set of 87 quasars. They derived that the Eigenvector1 (E1), driven by the anti correlation of the ratio R_{Fe} of equivalent width (EW) of FeII emission lines in the optical band and the FWHM of $H\beta$ emission line is the primary cause of variability in the parameters. Since then, various aspects of E1 involving a variety of data sets as well multi-frequency parameters have been discussed in multiple works (see Marziani et al., 2018, and references therein). Sulentic et al. (2000) and later Zamfir et al. (2010) established the foundations of the four-dimensional EV1 (4DE1) formalism, including the (FWHM) of $H\beta$ and R_{fe} as two of the main components. These two quantities are respectively related to the black hole mass and the Eddington ratio and these studies have resulted in the so called quasar main sequence (see Sulentic & Marziani, 2015; Marziani et al., 2018)

In this work, we have compiled a representative sample of NlSy1 galaxies and BlSy1 galaxies and performed a statistical study based on the various physical parameters responsible for driving the variations in both types of galaxies. The primary objective of current study is to understand the diversity observed in the physical parameters for a representative sample of both broad line and narrow line Seyfert-1 galaxies and its correlation with the physical parameters obtained through optical and X-ray observations, and then establish a comparison between the two types of galaxies based on these parameters.

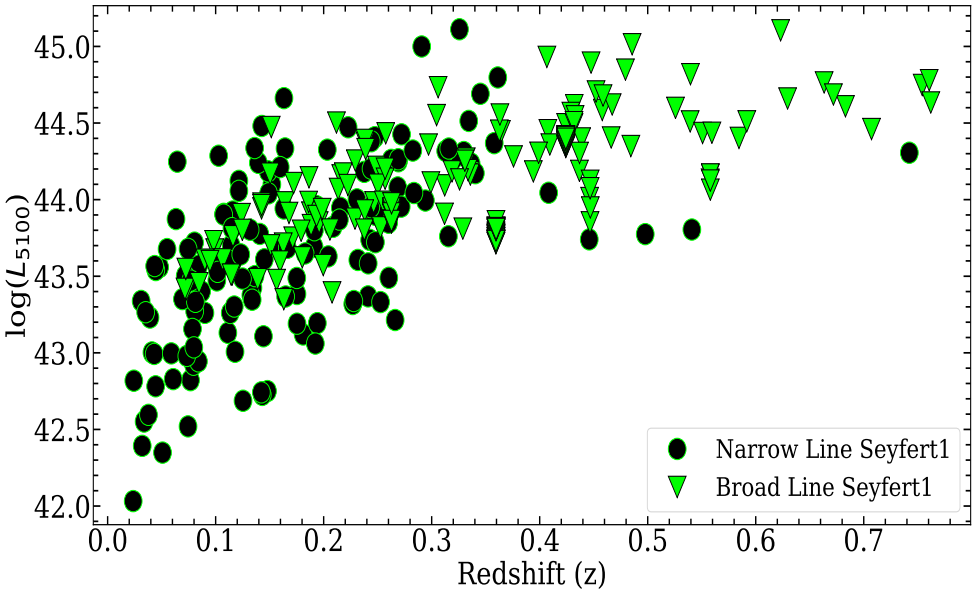

Figure 3.15: A representative sample of BlSy1(green triangle) and the NlSy1 galaxies (black circle) galaxies matching in luminosity and redshift (L-z) plane being used for this work. The limit of redshift is put at 0.8 for clear $H\beta$ emission line detection in SDSS.

3.6.2 Data and fitting procedure

A sample comprising of both BlSy1 and NlSy1 galaxies with almost similar luminosity and matching in the redshift domain has been assembled in order to study the properties of these two seemingly different classes of galaxies. More information about this sample is available in Ojha et al. (2020). The single epoch optical spectrum for all the sources was obtained from the SDSS archives (see York et al., 2000; Shen et al., 2011a; Rakshit et al., 2017, etc.) using the SDSS-SAS DR16 server[5]. For all the sources we performed a search query for the optical spectrum on the SDSS-SAS server for a region around 0.05 arc minutes within the specified Right Ascension (RA) and Declination (DEC) positions of these sources. The spectra were brought to the rest frame using the redshift values available in the header of the individual FITS files obtained from SDSS DR16. A limit of Signal to Noise Ratio (SNR) $\geq$

[5]https://dr16.sdss.org/optical/spectrum/search

5 was put for identifying the emission lines clearly. Out of the 225 NlSy1 galaxies in the sample, the SNR criteria reduced 10 sources while out of 164 BlSy1 galaxies from the sample, this criterion reduced 14 sources.

PyQSOFIT[6], a publicly available code to fit the quasar spectra has been used to analyse the individual spectra. It is written in Python language, and has been used for fitting the SDSS quasar spectra recently (see Rakshit et al., 2020; Gaur et al., 2019, etc.). Initially, the continuum model is prepared using the host galaxy components, contribution from the iron line and the accretion disk emission which reflects itself as a power law component (see Figure 3.16). We removed the host galaxy component using the PCA method, obtained from the host galaxy templates of (Yip et al., 2004) .For many of the sources in our sample the host galaxy decomposition could not be applied. The FeII blends were removed using the templates available in Boroson & Green (1992) which are available within the code itself. The accretion disk component was fitted as a polynomial and the final continuum model was subtracted from the original spectrum, which yielded the emission line components only. We were concerned with measuring the asymmetry in the $H\beta$ emission line, hence for the emission line fitting, we concentrated on the $H\beta$-OIII complex only. We assumed the emission line complex to be composed of a narrow and a broad central component representing the $H\beta$ emission arising from the Narrow line and Broad line regions respectively. The width of the narrow Gaussian components used for fitting the OIII doublet, was tied with the narrow component of the $H\beta$ emission line which physically indicates the emission coming from the same narrow line region. The limits for the width of the Gaussian profiles were set as 800 km/sec for narrow components, up to 2300 km/sec for broad components and beyond 10000 km/sec for very broad components for fitting the NlSy1 galaxies. The limit of 2300 km/sec was kept keeping in mind the previous works classifying the NlSy1 galaxies (for example,

[6]https://github.com/legolason/PyQSOFit

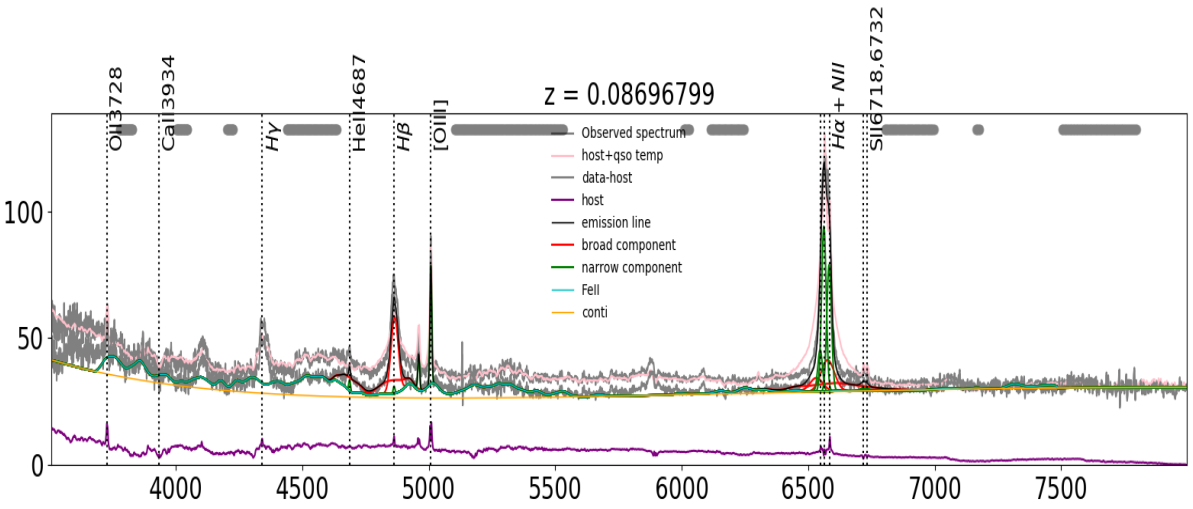

Figure 3.16: Demonstration of the fitting procedure using PyQSOFit. The continuum has been fit using a power law, the emission lines have been fit using a combination of gaussians, the host galaxy has been decomposed using already available tempelate in Yip et al. (2004) and the Fe blend has been removed using the tempelates available in Boroson & Green (1992).

see Rakshit et al., 2017). For fitting the BlSy1 we removed the upper limit of 2300 km/sec on the broad component, while still allowing up to three Gaussian profiles including a very broad component. Out of 225 NlSy1 galaxies, we could fit and get proper measurements of physical quantities for 144 sources, while out of 164 BlSy1 galaxies, we could fit and get proper measurements for 110 sources.

3.6.3 Analysis

We obtained the physical parameters from the spectral fitting and derived a few parameters based on empirical relations. The FWHM of the $H\beta$ emission line, area covered by the line, and its equivalent width (EW) were obtained from the direct decomposition of the spectra. The area covered by the $H\beta$ emission line was calculated by integrating the flux between 4700Åand 4920Å. We calculated the equivalent width (EW) of the emission line using the same wavelength window and the monochromatic luminosity at 5100 Å(L_{5100}) was obtained from the fit. The broad

line region of NlSy1 galaxies is understood to be richer in FeII content as compared to the general population (Panda et al., 2019). The iron strength (R_{Fe}) was calculated as the ratio of area covered by the broad Fe line between 4433Åand 4684Å, and the area covered by the $H\beta$ emission line.

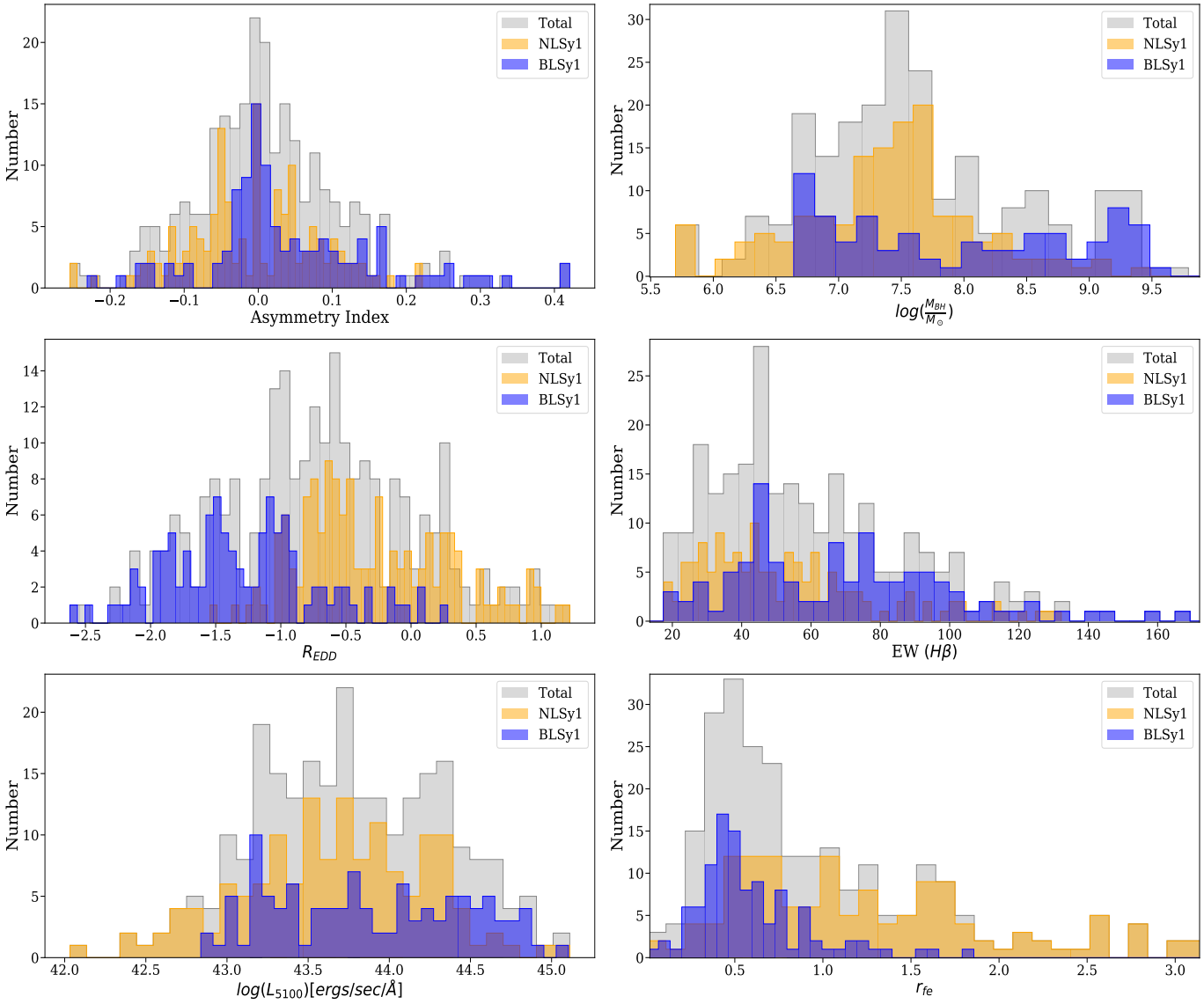

Figure 3.17: Distribution of various physical parameters for both the types of galaxies. Orange color denotes the NlSy1 galaxies, Blue color denotes the BlSy1 and the grey region is the combined number.

We found out the iron strength in NlSy1 galaxies to be higher than the BlSy1 galaxies for most of the AGN. The median R_{Fe} was 1.13 for the NlSy1 galaxies while

it was less than half of that value, 0.49 for the BlSy1 galaxies. We estimated the flux ratio of the narrow OIII component to the broad $H\beta$ in order to understand the influence of the $H\beta$ on the emission from NLR gases. The NlSy1 galaxies have weak OIII emission and thus the OIII/$H\beta$ ratio was lower compared to the BlSy1 galaxies. Also, the ratio of broad components of $H\alpha$ and $H\beta$ was calculated using the area covered by the broad components of the two emission lines.

The central black hole mass has been estimated using various empirical relations in the recent past. Reverberation mapping based masses provide tighter constraints on the Supermassive Black Hole (SMBH) mass and thus far this technique has been the only reliable one for SMBH mass estimation to higher redshifts (Bentz et al., 2009). The single epoch SMBH mass estimation technique is based on the scaling relations obtained from local galaxy stellar velocity dispersion.

$$M_{BH} = f_{BLR}\frac{R_{BLR}(\Delta v)^2}{G} \tag{3.7}$$

In this equation, R_{BLR} is the BLR radius in light days and is estimated using the so called Radius Luminosity (R-L) relation available for a set of approximately 120 reverberation mapped AGN so far (Bentz et al., 2009; Du & Wang, 2019), Δv is obtained from the FWHM of the emission line being used for the SMBH mass estimation, assuming that the gas is in virialized motion around the SMBH. The NlSy1 galaxies have smaller SMBH mass, owing to the small FWHM of the $H\beta$ emission line.

The NlSy1 galaxies have been known to have higher accretion rates as compared to the BlSy1, which makes it one of the defining parameters in the classification. These AGN are understood to be younger in age but accreting very fast. In the eigenvector formalism of Boroson & Green (1992), the Eddington ratio, $R_{Edd} = \frac{L_{BOL}}{L_{Edd}}$ is understood to drive the variations in the parameters. The Eddington ratio is also

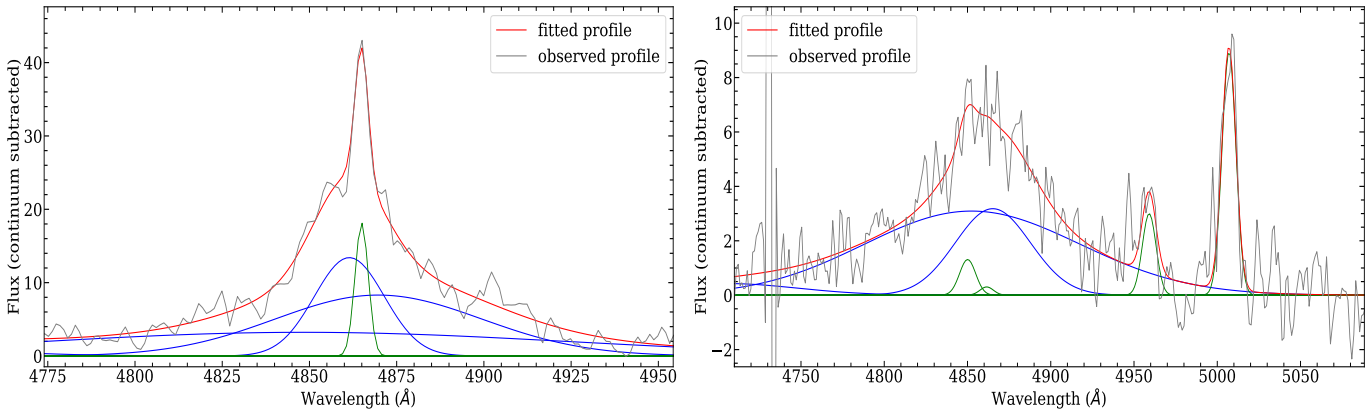

Figure 3.18: Example of blue (left) and red (right) asymmetric $H\beta$ profiles with AI values -0.14 and +0.12 respectively

interpreted as the age of the AGN in some recent works (Grupe, 2004). We estimated the Eddington ratio using optical spectra itself. In Ojha et al. (2020), R_{Edd} was calculated using X-ray observations which was consistent with the estimation from that obtained from optical parameters hence we did not attempt to estimate R_{Edd} using other methods.

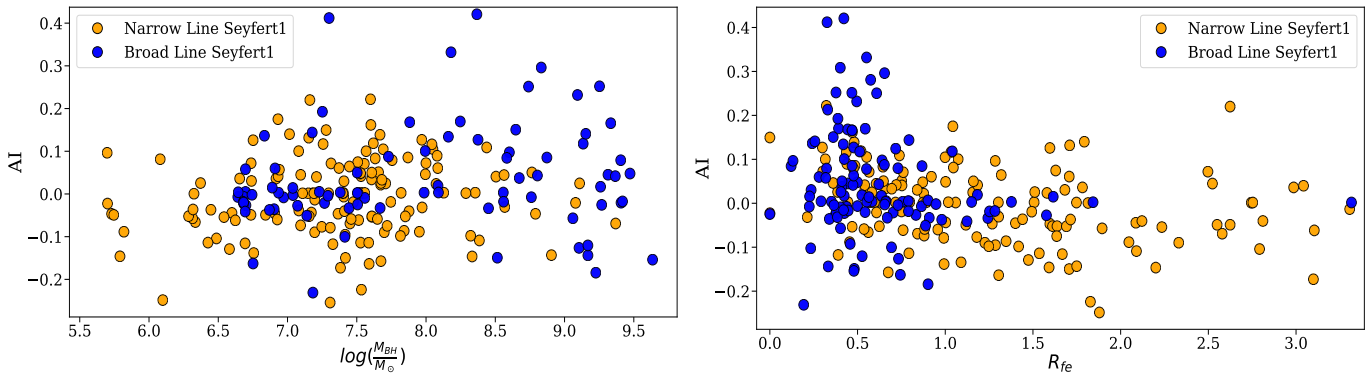

Figure 3.19: Correlation of asymmetry indices with Black hole mass and r_{fe} for NlSy1 (orange) and BlSy1 (blue) galaxies.

The asymmetry index has been used to trace the signatures of inflowing or outflowing gas in the broad line region of AGN. While the outflow asymmetry in the CIV line, known as the *blueshifting* is well known and documented (Gaskell & Goosmann, 2013) and possibly explained by the so called 2 component BLR model, the

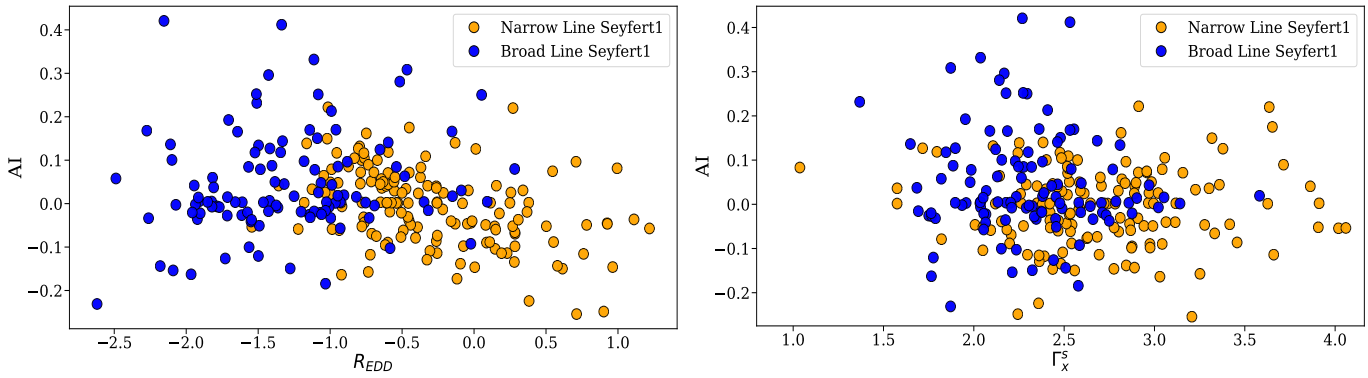

Figure 3.20: Correlation of asymmetry indices with R_{EDD} and Γ_x^s for NlSy1 (orange) and BlSy1 (blue) galaxies.

cause of similar asymmetry in a low ionisation line like $H\beta$ has not been known very well in the literature, although asymmetric $H\beta$ profiles have been known to exist. The characterisation of the AGN in terms of their emission line shapes and shifts and their correlation with physical parameters such as accretion rate etc. has been attempted in (Zamfir et al., 2010) where they conclude that the AGN with $H\beta$ FWHM $\geq$ 4000 km/sec show different characteristics than the ones with lower value of FWHM. We estimated the asymmetry indices for all the AGN in our sample. It has been calculated with different flux values in the recent past (Marziani et al., 1996; Brotherton, 1996). We chose a combination of 75% and 25% flux values to estimate the asymmetry index based on previous works. Basically the wavelength at which the broad emission line flux values reach the 75% and 25% of the flux values is recorded and the asymmetry index (AI) and Kurtosis Index (KI) are calculated. The correlation of AI with various physical parameters is shown in Figure 3.20. We also obtained the soft X-ray photon index as it is one of the fundamental components in the 4DE1 formalism. The X-ray photon indices were obtained from (Ojha et al., 2020). The comparison between X-ray photon indices and the BLR asymmetry provides clues to the connection of the corona in the accretion disk with the BLR. The distribution of the various parameters for the entire sample of BlSy1 and NLSy1 is

presented in Figure 3.17. To understand the correlation among the various derived parameters, we calculated the spearman rank correlation coefficients. It is a statistical technique used to find out the strength and the direction of the association between two variables.

3.6.4 Results

The direct correlations point to higher anti correlation of the $H\beta$ FWHM with R_{fe} and R_{Edd} in the NlSy1. While there is a strong anti correlation of FWHM with R_{fe} in both the cases, it is slightly weaker in the case of BlSy1 galaxies. This may be because of the fact that R_{fe} is strongly dependent on the flux of the iron emission line and thus the emission region of NLSy1 being richer in iron content as compared to the BlSy1. The Eddingtion ratio is anti correlated with the $H\beta$ FWHM with the anti correlation coefficient of -0.43 for the whole sample. When the correlation is calculated separately, a positive correlation of +0.33 is present in the case of BlSy1 while it is highly anti correlated with the FWHM of $H\beta$ in the case of NlSy1 galaxies, it's correlation coefficient being -0.84. Most of the NlSy1 galaxies have higher Eddington ratios but lower FWHM than the BlSy1 hence, this skews the results for entire population in the favour of NlSy1 galaxies in this analysis.

More NlSy1 galaxies show blue asymmetries as compared to the BlSy1, which seems quite interesting. Blue asymmetries means there is outflowing gas arising from that region. In the literature (see Panda et al., 2019; Wolf et al., 2020) it has been recently known that the NlSy1 galaxies show more traces of outflow. The FWHM of Hβ correlates positively, although weakly with the asymmetry index. The correlation coefficent is 0.26 in the case of BlSy1 galaxies while it comes out to be 0.37 in the case of NlSy1 galaxies. Also it is anti correlated with R_{Fe} in both the cases of NlSy1 galaxies and BlSy1 galaxies. There has been a postulation to use the AI in the emission profile as a surrogate parameter in the 4DE1 formalism.

The asymmetry index shows weak correlations and anti correlations with the other known parameters. Thus, we can't conclusively determine the asymmetry index to be a dominating factor in the AGN classification based on this analysis. Soft X-ray photon index has been one of the components of the 4DE1 formalism of Boroson & Green (1992) hence we tried to correlate it with other known parameters for this sample. Surprisingly, there is very weak correlation of the soft X-ray photon index with all the parameters in both the cases.

We tried to see if the differences in physical properties arise even when the NlSy1 galaxies are compared to the general Seyfert galaxies population. Naturally with the NlSy1 galaxies occupying extreme ends in some parameters space, it becomes imperative to understand the properties of these galaxies. In Grupe (2004), and more recently Ojha et al. (2020) and Waddell & Gallo (2020) the properties of NlSy1 galaxies have been studied comparatively with BlSy1 galaxies. In Grupe (2004), a sample of 110 X-ray selected galaxies was available, which is around 250 in our case, owing to the availability of SDSS sepctrum. The results between the two studies are largely consistent. We conclude from this work that the NlSy1 galaxies are richer in iron content (indicated by their high R_{fe} values), accrete very fast and show more traces of outflow, signified by their blue asymmetries.

Chapter 4

Conclusions

The aim of this project was to understand the sub parsec regions of Active Galactic Nuclei by applying the technique of reverberation mapping. To do it in a effective way, 8 narrow band filters were procured to catch the emission line flux. We calibrated the technique of reverberation mapping using spectroscopic data set. The photometric lags were in agreement with the spectroscopic lags, if the continuum contribution is taken into account. This, way we can use a combination of narrow band filters to catch the continuum and emission line flux. We have developed the tools to reduce and analyse the reverberation mapping data obtained from various telescopes. The tools for cross correlation analysis which include codes such as ICCF and JAVELIN have been well tested and their results have been compared well in order to optimize the technique being applied for reverberation mapping. The host galaxy contribution becomes important for nearby AGN. For this project too, it becomes important as the sources are located at lower redshift (z ¡ 0.1) and the contribution of the host galaxy flux can't be neglected in these cases, going by the literature. We have obtained the code: GALFIT for this purpose. GALFIT is a data analysis algorithm that fits 2-D analytic functions to galaxies and point sources directly to digital images. We have simulated multiple galactic profiles using analytic functions

available in the main program itself, and then inserted a Gaussian PSF representing the AGN as a point source. This exercise gives an idea about the host galaxy contribution to the incoming AGN flux, which we have to subtract in order to get the non contaminated AGN light curves. We run the simulations for various fractions of host galaxy contribution to the AGN flux and check for the effects on lag estimation. A comparative study which calibrated the results of Photometric reverberation mapping (PRM) with the traditional reverberation mapping has been done using Lick AGN Monitoring Project (LAMP) 2008 dataset and the results match quite well. This has helped us establish photometric reverberation mapping technique as a suitable, cost effective alternative to spectroscopic reverberation mapping.

We managed to get the reverberation lags and the BH mass estimates for a couple of AGN. We made use of the narrow band filters to get the H-b emission line flux. Using spectroscopy, we calculated FWHM of emission lines of our source MCG09 as 1917.456 ± 24.316 km/s means that these are broad emission lines coming from the BLR region. From virial relation, we also calculated black hole mass which is (2.87 ± 0.45) × 107 M . Based on commonly used R-L relation, we calculated black hole mass which is (2.97 ± 0.46) × 107 M and there is very much consistency between these two calculated black hole masses.

We observed a set of 5 AGN using the Thai Robotic Telescopes. The near-simultaneous photometric optical data of B, V, R and I band is used to determine the color diagram and the calculated lag between the broadband light curves is used to estimate the size of the accretion disk.The reduction and analysis of the data obtained is under progress. We will seek to verify the proposed relation between the inter band lags and the wavelength (R 4/3) obtained using the calculations of the standard Shakura Sunyaev disk, for our sample of AGN as well.

We have obtained the multiple band optical light curves from the Zwicky Transient Facility (ZTF) survey for a set of 120 quasars in order to get the accretion disk

structure for a large sample of quasar and complement our ongoing study. This is a high cadence, multiwavelength survey providing the data in 3 bands (g, r and i) for a large sample of northern sky objects which include a significant population of AGN. The accretion disk structure is obtained by estimating the reverberation lags between the gri band light curves. For this sample, as the central black hole masses are known through previous reverberation mapping campaigns, we are seeking the correlation between the BH mass and the accretion disk structure. Moreover, we're also looking at the correlation between the size of the accretion disk and the corresponding accretion rates of the AGN. This work is ongoing and is very important in our understanding of the inner structure of AGN accretion disks. It may be noted that the knowledge of the accretion disk structure for a large sample of quasars is lacking and only a handful of datasets are available.

A statistical study of the properties of NlSy1 and BlSy1 has been performed to yield clues to the peculiar behaviour of NlSy1 galaxies. We find out the the Narrow Line Seyfert galaxies are richer in iron content, have higher accretion rates and show traces of outflowing gas from their line emitting regions.

Chapter 5

Scope of future work

The main aim of the project was to collect the data and analyze it for the estimation of Broad line region size and the black hole mass for a sample of low luminosity AGN for the first time in a systematic way. Due to limited time frame an optimal representative sample has been covered. This sample will be enhanced in future, based on the methodology developed in this project and the experimental setup such as a set of narrow-band calibrated redshift filter established in this project. We are continuing the monitoring of the AGN in our sample in the ongoing observation cycle. Data gathered in this project by now and that flowing-in the near future should be archived for the use of AGN community

As we are equipped with high cadence, long duration light curves of a large sample of AGN , thanks to the monitoring done using the NARIT and Devasthal telescopes and complemented by the ZTF dataset, the modeling of the quasar light curves for a large population of quasars to understand the drivers of AGN variability will be done. The variability of the quasars has been proposed as a Damped Random Walk (DRW) or in other terms an Ornstein Uhlenbeck (OU) process for timescales longer than a few days. A white noise power spectral density (PSD) is expected at low frequency in this model; however, a direct observational constraint to the low-frequency PSD

slope is difficult due to the limited lengths of the light curves available. Previous studies have suggested that quasar variability amplitude increases with decreasing luminosity, rest frame wavelength, and Eddington ratio, and increases with increasing black hole mass. We are developing the models in order to understand the physical drivers behind the variability of quasars.

We are analysing the light curves obtained from the Zwickey transient facility (ZTF) as part of our broader goal of understanding the inner disk structure for a large number of quasars. This is an ongoing work with the initial results being promising and we are expecting really exciting results from this work. With the future installation of the facilities such as the Large Synoptic Survey Telescope (LSST), the knowledge gained through this research project will be really helpful as we are working on the similar lines of high cadence long term monitoring of AGN.

The 8 redshifter narrow band H-alpha and H-beta wavelength filters have become a very important asset for the Devasthal observatory and they are being used as part of a new instrument ADFOSC (see Omar et al, aXiv ID:1908.02531) mounted on the 3.6m DOT for narrow band imaging of certain galaxies apart from the ongoing photometric reverberation mapping project using 1.3m DFOT. Narrow band imaging of the edge-on galaxies can be helpful in understanding the ionisation cones related to the outflowing OIII gas from the inner regions of these AGN. Further, the H-alpha narrow band imaging is helpful in estimating the star formation rates in galaxies. Since the 8 narrow band filters cover a vast span of redshifts the studies can be done for larger samples at once. Some of these exciting projects have already been proposed in the ongoing and upcoming cycles of 3.6m DOT which has been made possible with the availability of narrow band filters at the Devasthal observatory.

Chapter 6

S&T benefits accrued

6.1 List of publications

1. Broadband reverberation mapping of 5 AGN using Thai Robotic Telescopes. Vivek Kumar Jha, Hum Chand, Ravi Joshi et al. 2022 *in preparation*

2. Evidence of Jet induced Optical Microvariability in Radio-loud Narrow Line Seyfert 1 Galaxies. Vineet Ojha, Vivek Kumar Jha, Hum Chand, Veeresh Singh, 2022. *Accepted for publication in Monthly Notices of the Royal Astronomical Society (DOI: stac1627).*

3. Accretion Disk Sizes from Continuum Reverberation Mapping of AGN Selected from the ZTF Survey. Vivek Kumar Jha, Ravi Joshi, Hum Chand, Xue-Bing Wu, Luis C Ho, Shantanu Rastogi, Quinchun Ma; 2022. *Monthly Notices of the Royal Astronomical Society, 511, 2.*

4. A comparative study of the physical properties for a representative sample of Narrow and Broad-line Seyfert galaxies. Vivek Kumar Jha, Hum Chand, Vineet Ojha, Amitesh Omar and Shantanu Rastogi; 2021. *Monthly Notices of the Royal Astronomical Society, 510, 3*

5. Properties of Broad and Narrow Line Seyfert galaxies selected from SDSS. Vivek Kumar Jha, Hum Chand, and Vineet Ojha. *Communications of the Byurakan Astrophysical Observatory (ComBAO), Volume 67, Issue 2, December 2020.*

6. Probing the central engine and environment of AGN using ARIES 1.3-m and 3.6-m telescopes; Hum Chand et. al. 2018, *BSRSL, 87, 291C*

6.2 Manpower trained

Two Ph.D students registered for their thesis under this project:

- **Mr. Krishan Chand** registered for a Ph.D degree in 2018 at Kumaun University.

- **. Mr. Vivek Kumar Jha** registered for a Ph.D degree in 2019 at Deen Dayal Upadhyayay Gorakhpur university. Thesis title: **Investigating the nature and structure of Broad Line region in Active Galactic Nuclei**

6.2.1 Patents Filed

NIL

6.3 Financial position

Item	Sanctioned amount	Received amount	Expenditure		Balance
Non recurring	grant:				
Equipments	24,22,780	24,22,780	23,14,491		1,08,289
Recurring	grant:				
Manpower/	13,29,600	1,00,000	6,97,000	JRF salary (till March 2020)	91,196
travel/		3,00,000	20,235	Contingency	
contingencies		6,00,000	1,97,667	JRF Salary (committed)	
		1,06,098 interest		for March-Sep 2020	
Overhead	3,00,190		1,00,000	Overhead	
Total	40,52,570	35,28,878	33,29,393		1,99,485

Figure 6.1: Financial condition. All the amounts are in INR.

Bibliography

Abazajian, K. N., Adelman-McCarthy, J. K., Agüeros, M. A., et al. 2009, , 182, 543

Bahcall, J. N., Kozlovsky, B.-Z., & Salpeter, E. E. 1972, Astrophys. J., 171, 467

Bahcall, J. N. J., Kozlovsky, B.-Z. B.-Z., & Salpeter, E. E. 1972, Astrophys. J., 171, 467

Barth, A. J., Bennert, V. N., Canalizo, G., et al. 2015, The Astrophysical Journal Supplement Series, 217, 26

Bellm, E. C., Kulkarni, S. R., Graham, M. J., et al. 2019, , 131, 018002

Bentz, M. C. 2015, Astronomy at High Angular Resolution, 439, arXiv:1505.04805

Bentz, M. C., & Katz, S. 2015, Publ. Astron. Soc. Pacific, 127, 67

Bentz, M. C., Peterson, B. M., Netzer, H., Pogge, R. W., & Vestergaard, M. 2009, Astrophys. J., 697, 160

Bentz, M. C., Denney, K. D., Cackett, E. M., et al. 2006, The Astrophysical Journal, 651, 775

Bentz, M. C., Walsh, J. L., Barth, A. J., et al. 2010, Astrophys. J., 716, 993

Bentz, M. C., Denney, K. D., Grier, C. J., et al. 2013, Astrophysical Journal, 767, arXiv:1303.1742

Blandford, R. D., & McKee, C. F. 1982, Astrophys. J., 255, 419

Bon, E., Zucker, S., Netzer, H., et al. 2016, Astrophys. J. Suppl. Ser., 225, 29

Boroson, T. A., & Green, R. F. 1992, Astrophys. J. Suppl. Ser., 80, 109

Brotherton, M. S. 1996, THE PROFILES OF Hß AND [O III] X5007 IN RADIO-LOUD QUASARS, Tech. rep.

Bruzual, G., & Charlot, S. 2003, , 344, 1000

Chand, H., Rakshit, S., Jalan, P., et al. 2018, Bull. la Soc. R. des Sci. Liege, 87, 291

Chelouche, D., & Daniel, E. 2012, Astrophysical Journal, 747, arXiv:1105.5312

Czerny, B. 2019, Open Astron., 1, arXiv:1908.00742

De Rosa, G., Peterson, B. M., Ely, J., et al. 2015, Astrophys. J., 806, 128

Du, P., & Wang, J.-M. 2019, The Astrophysical Journal, 886, 42

Du, P., Hu, C., Lu, K.-X., et al. 2014, Astrophys. J., 782, 45

—. 2015

Du, P., Lu, K.-X., Zhang, Z.-X., et al. 2016, Astrophys. J., 825, 126

Du, P., Zhang, Z.-X., Wang, K., et al. 2018, Astrophys. J., 856, 6

Edri, H., Rafter, S. E., Chelouche, D., Kaspi, S., & Behar, E. 2012, Astrophysical Journal, arXiv:arXiv:1206.4486v1

Fausnaugh, M. M., Grier, C. J., Bentz, M. C., et al. 2017a, \apj, 840, 97

—. 2017b, Astrophys. J., 840, 97

Gaskell, C. 2000, New Astronomy Reviews, 44, 563

Gaskell, C. M., & Goosmann, R. W. 2013, Astrophys. J., 769, 30

—. 2016, Astrophys. Space Sci., 361, 67

Gaur, H., Gu, M., Ramya, S., & Guo, H. 2019, Astronomy & Astrophysics, 631, A46

Goad, M. R., Korista, K. T., & Ruff, A. J. 2012, , 426, 3086

Gourgouliatos, K. N., & Komissarov, S. S. 2018, Nat. Astron., 2, 167

Grier, C. J., Trump, J. R., Shen, Y., et al. 2018, arXiv:1711.03114v3

Grier, C. J., Shen, Y., Horne, K., et al. 2019, ArXiv e-prints, arXiv:1904.03199

Grupe, D. 2004, The Astronomical Journal, 127, 1799

Guo, H., Shen, Y., & Wang, S. 2018, PyQSOFit: Python code to fit the spectrum of quasars, Astrophysics Source Code Library, ascl:1809.008

Haas, M., Chini, R., Ramolla, M., et al. 2011, Astronomy & Astrophysics, 535, A73

Hemler, Z. S., Grier, C. J., Brandt, W. N., et al. 2019, Astrophys. J., 872, 21

Homayouni, Y., Trump, J. R., Grier, C. J., et al. 2018, ArXiv e-prints, arXiv:1806.08360

Kaspi, S., Smith, P. S., Netzer, H., et al. 2002, Astrophys. J., 533, 631

Kellermann, K. I. 2014, J. Astron. Hist. Herit., 17, 267

Kelly, B. C., Bechtold, J., & Siemiginowska, A. 2009, Astrophysical Journal, 698, 895

King, A. L., Martini, P., Davis, T. M., et al. 2015, \mnras, 453, 1701

Kovacevic, J., Popovic, L. C., & Dimitrijevic, M. S. 2010, VizieR Online Data Catalog, J/ApJS/189/15

Li, Y.-R., Wang, J.-M., & Bai, J.-M. 2016, The Astrophysical Journal, 831, 206

Lyke, B. W., Higley, A. N., McLane, J. N., et al. 2020, , 250, 8

MacLeod, C. L., Ivezić, Ž., Kochanek, C. S., et al. 2010, Astrophysical Journal, 721, 1014

Mandal, A. K., Rakshit, S., Kurian, K. S., et al. 2018, Mon. Not. R. Astron. Soc., 475, 5330

Marziani, P., Sulentic, J. W., Dultzin-Hacyan, D., Calvani, M., & Moles, M. 1996, Astrophys. J. Suppl. Ser., 104, 37

Marziani, P., Dultzin, D., Sulentic, J. W., et al. 2018, Frontiers in Astronomy and Space Sciences, 5, 6

Mathur, S. 2000, , 44, 469

Merloni, A. 2016, Observing Supermassive Black Holes Across Cosmic Time: From Phenomenology to Physics, Vol. 905, 101

Meyer-Hofmeister, E., Liu, B. F., & Qiao, E. 2017, Interaction of the accretion flows in corona and disk near the black hole in AGN, Tech. rep., arXiv:1712.02031v1

Mudd, D., Martini, P., Zu, Y., et al. 2018, The Astrophysical Journal, 34, 123

Netzer, H. 2008, New Astron. Rev., 52, 257

—. 2015, Annu. Rev. Astron. Astrophys., 53, 365

—. 2018, Frontiers in Astronomy and Space Sciences, 5, 1

Netzer, H., & Peterson, B. M. 1997, arXiv:9706039 [astro-ph]

Nuñez, F. P., Chelouche, D., Kaspi, S., & Niv, S. 2017, Publ. Astron. Soc. Pacific, 129, 094101

Ojha, V., Chand, H., Dewangan, G. C., & Rakshit, S. 2020, arXiv:2005.08352

Ojha, V., Chand, H., Krishna, G., Mishra, S., & Chand, K. 2020, , 493, 3642

Padovani, P. 2017, Frontiers in Astronomy and Space Sciences, 4, 1

Padovani, P., Alexander, D. M., Assef, R. J., et al. 2017, Astronomy and Astrophysics Review, 25, arXiv:1707.07134

Panda, S., Marziani, P., & Czerny, B. 2019, , 882, 79

Patterson, M. T., Bellm, E. C., Rusholme, B., et al. 2019, , 131, 018001

Peterson, B. M. 1999, in Astronomical Society of the Pacific Conference Series, Vol. 175, Structure and Kinematics of Quasar Broad Line Regions, 49

Peterson, B. M., & Horne, K. 2004, 325, 248

Peterson, B. M., Wanders, I., Horne, K., et al. 1998, On Uncertainties in Cross-Correlation Lags and the Reality of Wavelength-dependent Continuum Lags in Active Galactic Nuclei, Tech. rep.

Pozo Nuñez, F., Ramolla, M., Westhues, C., et al. 2012, AA, 545, A84

Rakshit, S., & Stalin, C. S. 2017, Astrophys. J., 842, 96

Rakshit, S., Stalin, C. S., Chand, H., & Zhang, X.-G. 2017, Astrophys. J. Suppl. Ser., 229, 39

Rakshit, S., Stalin, C. S., & Kotilainen, J. 2020, The Astrophysical Journal Supplement Series, 249, 17

Ramolla, M., Pozo Nuñez, F., Westhues, C., Haas, M., & Chini, R. 2015, The stability of the optical flux variation gradient for 3C 120, Tech. rep., arXiv:arXiv:1508.01723v2

Ramos Almeida, C., & Ricci, C. 2017, arXiv:1709.00019v1

Schmidt, M. 1963, Nature, 197, 1040

Shakura, N. I., & Sunyaev, R. A. 1973, , 500, 33

Shen, Y., Richards, G. T., Strauss, M. A., et al. 2011a, , 194, 45

—. 2011b, , 194, 45

Shen, Y., Hall, P. B., Horne, K., et al. 2015, arXiv:1810.01447v1

Shen, Y., Grier, C. J., Horne, K., et al. 2019, arXiv:1908.00027

Smee, S. A., Gunn, J. E., Uomoto, A., et al. 2013, , 146, 32

Starkey, D. A., Horne, K., & Villforth, C. 2016, MNRAS, 456, 1960

Stetson, P. B. 1987, , 99, 191

Sulentic, J. W., & Marziani, P. 2015, Frontiers in Astronomy and Space Sciences, 2, 6

Sulentic, J. W., Zwitter, T., Marziani, P., & Dultzin-Hacyan, D. 2000, , 536, L5

Sun, M., Xue, Y., Cai, Z., & Guo, H. 2018, arXiv:1803.06090

Tadhunter, C. 2008, New Astron. Rev., 52, 227

Véron-Cetty, M., & Véron, P. 2000, Astron. Astrophys. Rev., 10, 81

Waddell, S. G. H., & Gallo, L. C. 2020, , 498, 5207

Walsh, J. L., Minezaki, T., Bentz, M. C., et al. 2009, , 185, 156

Wang, J. M., Du, P., Hu, C., et al. 2014, Astrophysical Journal, 793, arXiv:1408.2337

Wang, S., Shen, Y., Jiang, L., et al. 2019, arXiv:1903.10015

Wolf, J., Salvato, M., Coffey, D., et al. 2020, Mon. Not. R. Astron. Soc., 492, 3580

Yip, C. W., Connolly, A. J., Szalay, A. S., et al. 2004, , 128, 585

York, D. G., Adelman, J., Anderson, John E., J., et al. 2000, , 120, 1579

Yu, Z., Martini, P., Davis, T. M., et al. 2018, Quasar Accretion Disk Sizes from Continuum Reverberation Mapping in the DES Standard Star Fields, Tech. rep.

Yue, M., Jiang, L., Shen, Y., et al. 2018, Astrophys. J., 863, 21

Zamfir, S., Sulentic, J. W., Marziani, P., & Dultzin, D. 2010, Mon. Not. R. Astron. Soc., 403, 1759

Zhang, H., Yang, Q., & Wu, X.-B. 2017a, Astrophys. J., 853, 116

—. 2017b, \apj, 853, 116

Zhang, X.-G. 2014, , 438, 557

Zu, Y., Kochanek, C. S., Kozłowski, S., & Peterson, B. M. 2013, 122, arXiv:1310.6774

Zu, Y., Kochanek, C. S., & Peterson, B. M. 2011, The Astrophysical Journal, 735, 80